Skiron : A beamline for Advanced Chiroptical Spectroscopies

Oriol Arteaga , Josep Nicolás and Salvador Ferrer

October 2014

Abstract :

We propose a bending magnet beamline, Skiron, for advanced chiroptical spectroscopies in solids, liquids and gases. Two different branches will address different experimental scenarios:

Branch A (windowless, in vacuum) will deliver monochromatic circularly polarized photons in the wavelength range 400- 30 nm (3-40 eV) with helicity switching frequency of ~1 kHz. Circular Dichroism (CD) will be probed by measuring differences of the photoemitted electron currents from a gas or liquid jet. As a result, CD spectroscopy in a unprecedented energy range will be possible, allowing to explore the optical activity of electronic transitions involving deep molecular orbitals of relevant organic molecules.

Branch B will deliver photons in the interval 400- ~130 nm. It will use linearly polarized radiation from the bending magnet and a recent instrumental development based on four photoelastic modulators which will allow to measure in real time the complete Mueller polarization matrix of solutions, solids or thin films and , in his way, to simultaneously determine the linear and circular dichroism of anisotropic systems.

Contents

1.- Introduction

1.1 Historical notes . [1]

Chirality is a ubiquitous phenomenon through nature ranging from fundamental particles, molecules, solutions, crystals, living organisms to galaxies. Chirality is closely linked to optical activity and chiroptical spectroscopies refer to the response of chiral objects to polarized electromagnetic radiation. Nearly all biomolecules, and pharmaceutical products are chiral and are the object of chiroptical spectroscopies. A chiral molecule and its mirror image are non-superposable and, in chemistry, each one of these two forms is called an enantiomer.

The discovery of optical activity is attributed to two French scientists Dominique-Francois Jean Arago (1786-1853 of Catalan origin) and Jean Baptiste Biot (1774-1862) which observed the rotation of the plane of polarization of light that traversed a quartz crystal. The chirality of quartz crystals arises from the helical arrangement of Si and O tetrahedrons in SiO2 crystals. Both scientists investigated the optical activity of quartz crystals although Biot also investigated organic compounds as oils and solutions of sugar and tartaric acid. Later, Adam Arnster at the end of the XIX century discovered that the angle of rotation was dependent of the wavelength of the radiation and exhibited a maximum. This was named optical rotary dispersion. In 1895 the 26 year old Aime' August Cotton , PhD student of l'Ecole Normale Superieur discovered that the rotation angle may show a maximum and a minimum at different wavelengths and that in between, the ellipticity exhibits a maximum. Cotton introduced the term "circular dichroism" (CD) to refer to this phenomenon. In 1940 , circularly polarized luminescence was observed from chiral crystals. In 1950, commercial instruments were fabricated to measure the optical rotation and in 1960 instruments for measuring the electronic circular dichroism were introduced which originated a large expansion of chiroptical spectroscopies in the fields of organic and inorganic chemistry and biochemistry. In the decade of 1970 other dichroic effects were observed in addition to the electronic CD (that results from electronic transition from filled to empty states upon absorption of a photon): vibrational CD and Raman optical activity However, in this manuscript we will only refer to electronic CD.
The quantum mechanical description of the chiroptical phenomena dates from 1929 by Rosenfeld [2], in 1948 the exciton theory for UV was published (Davydov) [3] but only until 1980-90 he theoretical descriptions did not reach a mature stage.
In Spain instruments for CD measurements in solutions and thin films are widespread in many universities and laboratories. At present there are at least 30 equipments devoted to CD . The first one dates from 1990 approximately.

1.2 Basic Concepts

Linearly polarized light may be regarded as arising from the superposition of two circularly polarized waves. If the light propagates in an anisotropic medium that introduces a phase shift δ to the right circularly polarized wave and –δ to the left then, the plane of polarization is turned an amount δ . If the phase shift δ is due to different refraction index n of both circular polarizations then for a medium of thickness d , $2\delta = k(n_l - n_r)d$, being k the magnitude of the wavevector . The rotation of the plane of polarization per unit length δ/d is the so called rotatory power or rotary dispersion R which is directly related to the difference of the refraction index.
On the other hand, a different effect, CD arises if the absorption of both circular polarized waves is different. If a linearly polarized light transverses a medium of thickness d that has dichroism (different absorption coefficients a_r and a_l) , the amplitudes of the circularly polarized waves are different at the exit which results in an elliptical polarized light. The ratio of the two axes of the ellipse is directly related to the difference in absorption of right and left polarizations and defines the so called ellipticity $\Delta\varepsilon = ¼ (a_l - a_r)d$ [4] .

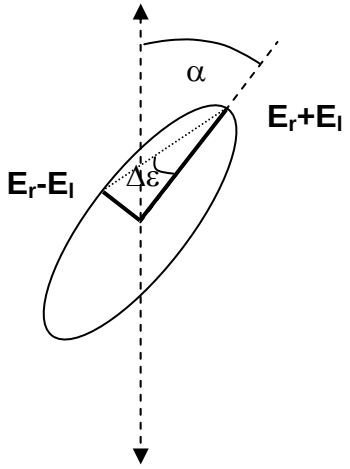

Figure 1.1 :

The difference of refraction index for right and left circularly polarized light originates the rotation α of the ellipse that describes the electric vector. The difference in absorption coefficients causes different magnitudes of $\mathbf{E_r}+\mathbf{E_l}$ and $\mathbf{E_r}-\mathbf{E_l}$ which determine the ellipticity angle Δε.

Moreover, rotary power and ellipticity are closely related to each other through Krammers-Kronig transforms, which allows to convert one into the other :

$$R \propto \int \frac{\Delta\varepsilon(\lambda)}{\lambda} d\lambda$$

where the integral extends to the whole range of available wavelengths.
As a consequence in many cases the discussions on optical activity refer indistinctly to rotary power or dichroism.

The quantum mechanical description of the rotary power derived by Rosenfeld [2] demonstrated that the rotary power is equal to the imaginary part of the scalar product between the electric transition moment and the magnetic transition moment:

$$R = \mathrm{Im}\left\{\langle 0/p/a\rangle \bullet \langle a/m/0\rangle\right\}$$

Where 0 and a refer to initial and final states and p and m are the electric dipole and magnetic dipole operators. In classical terms, the above results states that the projection of the induced electric dipole arising from the dipolar electric transition, originated by the absorption of a photon, on the induced magnetization has to be non zero to have optical activity in the absorption band among the states 0 and a. [5].
The expression of R corresponds to a second order effect involving dipolar electric and magnetic transitions. In many practical cases R arises from dipolar forbidden electrical transitions that become sizeable due to the effect of the electronic neighborhood of the absorbing atom. What matters here is that in many cases CD defined from the experimentally measured transmissions of left and right circularly polarized light rays $(I_r-I_l)/(I_r+I_l)$ is of the order of 10^{-4} or even 10^{-5}. For comparison, X ray magnetic CD in transition metals as Fe, Co and Ni is of the order of 10^{-1}.

The electronic CD exciton chirality method [6] allows to determine the absolute configuration of chiral compounds in a non empirical manner without referring to model compounds with known configuration. Suppose that a chiral compound has two cromophores that absorb a photon each one via , for example , an allowed dipolar transition π to π^* . The electrical dipoles induced by the absorption of the light interact with the electrostatic dipole-dipole energy which generates and additional energy term in the Hamiltonian which splits the final state in two one sublevels with positive and negative rotary dispersions:

$$R \propto \pm \boldsymbol{r}_{ij} \bullet (\boldsymbol{p}_{i0a} \times \boldsymbol{p}_{j0a})$$

r_{ij} is the vector from the i to the j chromophores and $p_{i,j0a}$ refers to the induced electric dipole moment in the chromophores for an optical absorption transition from 0 to a.
The sign of the rotary power depends on the configuration of the chromophores and the orientation of their induced dipoles.
Experimentally the interaction of both dipoles results in the so called bisignate intense CD Cotton signal which sign reflects the arrangements of the two cromophores in the compound.

The exciton model is extensively used in the literature to rationalize the CD spectra of organic compounds in solutions including biomolecules.

As mentioned above the rotary power is usually small since it arises from a second order effect. Due to its smallness, electronic CD measurements based on differential photon absorption are inherently difficult in dilute systems and necessitate relatively thick samples to achieve sizeable signals. In solutions of biological systems the pathlengths within the samples are typically around 0.1 mm or more.

Almost 40 years ago B. Ritchie [7] published a theoretical paper demonstrating that in randomly oriented molecules exhibiting optical activity (dextrorotatory or levorotatory), the angular distribution of emitted photoelectrons ejected on absorption of left or right polarized light has a term that is sensitive to the chirality of the emitting molecule:

$$I(\theta) = \frac{\sigma}{4\pi}\left[1 - \frac{\beta}{2}\left(\frac{3}{2}\cos^2\theta - \frac{1}{2}\right) \pm B\cos\theta\right]$$

The angle θ is defined by the direction of the photon beam and the emitted phtoelectrons ,σ is the photoelectric cross section and the coefficients β and B contain coupling terms in combination with photoionization matrix elements. The plus and minus sign of the B term , introduced by Ritchie, respectively refer to the emission from dextro or levorotatory randomly oriented molecules which exhibit different photoemission yields for a given θ. Alternatively, a given enantiomer exhibits a difference in the photoemission current at θ and θ+π equal to 2Bcosθ, being B directly related to the optical activity
The quadratic term in cosθ vanishes at the so called magic angles: $\theta m = \cos^{-1}(1/\sqrt{3}) = 54.7^\circ$ and $180^\circ + \theta m = 234.7^\circ$.

Most important is the fact that the magnitude of B is the result of a first order effect based on the interference of dipolar transition matrix elements associated to the absorption of the photons and consequently its magnitude was predicted to be orders of magnitude larger that the conventional natural electric/magnetic dichroism. In recent literature this effect is named PECD (photoemission circular dichroism).

The prediction by Ritchie was brought to evidence 25 years later, in 2001, by the group of Heizmann [8] wich measured using circularly polarized radiation from a bending magnet at Bessy, normalized differences of the photocurrents from gas phase camphor molecules as high as 0.04.

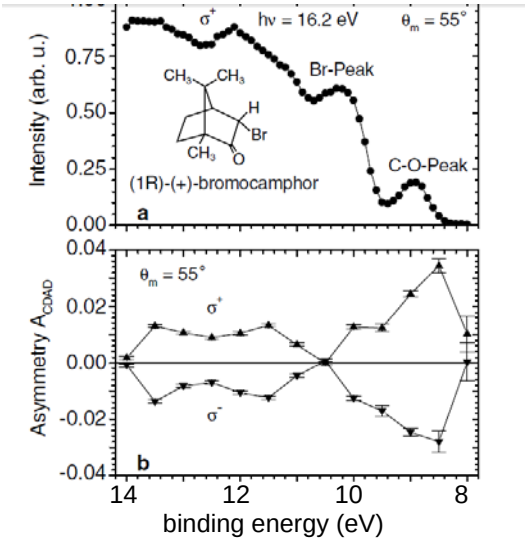

Figure 1.2.-

From ref. 8 . Upper panel
Gas phase photoemission from (+)bromocamphor from incident photons of energy 16.2 eV.

Bottom panel : normalized asymmetry of the photocurrents at angle of 55 and 55+180 degrees from the incoming photon beam. σ+ and σ - refer to positive and negative photon helicities of the circularly polarized radiation generated from a bending magnet source at Bessy I.

1.3 Selected examples of chiral spectroscopy.

1.3.1 Secondary structures of proteins

The most extended application of CD spectroscopy is probably in the analysis of solutions of biomolecules, particularly for studying protein secondary structures. This application has been active for more than two decades. Empirical analyses rely on the availability of reference data sets of far UV CD spectra of proteins whose crystal structures have been determined. An extensive research for defining a data set has been performed by the group of Wallace and co-workers [9]. As an example to illustrate how spectra typically look line , figure 1.3 displays the 72 spectra of proteins of the SP175 data set.

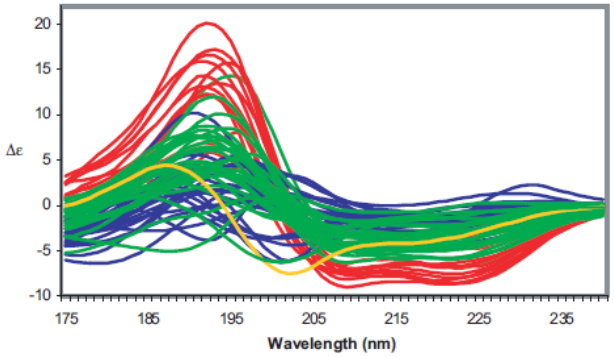

Figure 1.3.

CD spectra of all the component proteins of the data base. The spectra of the mainly α-helical proteins are in red, the mainly β-sheet in blue , the mixed helical/sheet in green and the " other" are in yellow [9].

It is interesting to notice that at the lowest measured wavelength, the red spectra have positive values while the blue are negative.
It is clear form the figure that very careful data fitting procedures and error analysis are required to decompose a CD spectrum measured in an undetermined sample into one of several reference spectra.

1.3.2 Chiral amplifiers.

Chirality amplifiers are designed and utilized to sense chirality in molecules with weak optical activity. By linking zinc porphyrines which have flexible parts in their structure with chiral diamines or alcohols a large enhancement of CD may be obtained since the porphyrine-diamine (or alcohol) complex produce bisignate CD signals resulting from the interaction of excitons of the twisted porphyrine transitions. Figure 1.4 from ref. 6 , chap.9, shows in panel a the Zn porphyrine which may have two conformations: either the left half in above the right or viceversa. Both conformations result in different signs of the CD as described by the exciton model. The diamine in panel b ,linked to the porphyrine produces an intense CD signal (panel c) of more than 1000 cm^{-1} mol^{-1}.

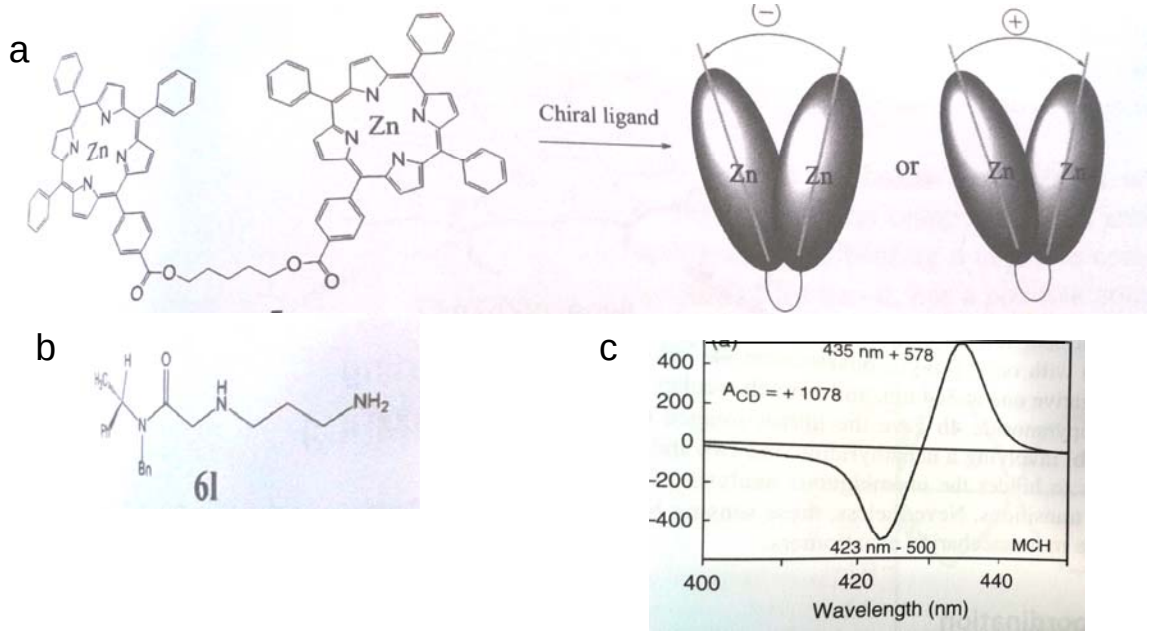

Figure 1.4.

(a): zinc porphyrines may adopt two configurations upon binding with a chiral ligand. They resemble scissors either right or left handed. (b) diamine ligand. (c) ellipticity $\Delta\varepsilon$ in $cm^{-1}(mol/liter)^{-1}$ versus wavelength. The intense bisignated CD is a consequence of the interaction of the excitons.

1.3.3 Supramolecular systems

Supramolecular structures rely on the formation of intermolecular bonds through a large variety of interactions as electrostatic, hydrophobic, hydrogen bonding, Van der Vaals, adsorption …The understanding of the intermolecular , non covalent, bonds is much less advanced than the covalent bond formation but those are responsible of the formation of supramolecular species some of them exhibiting conformational switching upon given particular stimuli as temperature and light. Supramolecular structures may be chiral even if the building blocks are achiral, and a given chirality can be transformed to the enantiomeric by external stimuli.[10]. These phenomena exhibit an enormously rich and important phenomenology that allows to gain understanding of complex systems. The creation, control and amplification of chirality is a fundamental issue in biosciences and material science.

A nice and representative example of supramolecular transformations is depicted in figure 1.5 which illustrates a molecular motor driven by light and temperature [11].

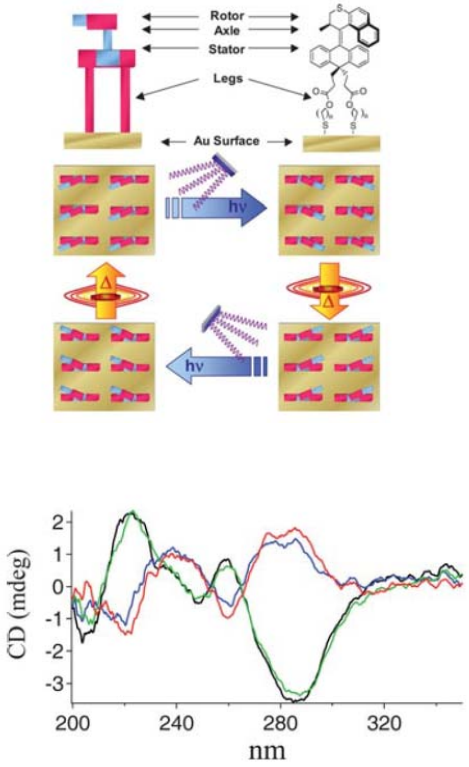

Figure 1.5.-

The thiol molecular layer, di-sulphur terminated, was adsorbed on a very thin film of Au (5nm) deposited on a coated quartz substrate. The S-Au bond is strong enough to have the "legs " of the thiol molecule firmly anchored on the metal. The head of the thiol is connected to the rest of the molecule by an axis that allows its rotation with a proper stimulus. The surface concentration of thiol molecules was about 10^{14} cm^{-2} . The initial spectrum (black) shows an inversion of the signal when the enantiomer is generated (red) by means of UV irradiation.

Thermal helix inversion (60 ˚C , 2 h) restores the initial spectrum (green). A second photochemical isomerization (blue) generates the second unstable enantiomer in the rotary cycle. Subsequent thermal treatment regenerates the original conformation [11].

1.3.4 Photon induced deracemization.

The different absorption of right and left circularly polarized radiation by chiral molecules may result in the evolution, upon irradiation, of an initially racemic mixture(i. e. one that has equal amounts of left- and right-handed enantiomers of a chiral molecule) towards an enrichment of one enantiomer over the other. The first evidence of this phenomenon was published in 1974 by Yoneda et al. [12] . Irradiation of a racemic Cr-acetyl-based solution with circularly polarized light obtained form a laser and a quarter wave plate resulted on a 4.5 % enrichment of an enatiomer over the other. Which enantiomer was enriched depended on the helicity of the radiation.
This phenomenon attracted considerable research over the last years and it has been even argued that could be in the origin of the homochirality of aminoacids and sugars in living organisms [13].
A recent result illustrates the richness of the phenomena participating in the photon induced processes. An initial racemic solution of crystallites with R and L crystal

structures evolved to a 100% pure R or pure L by irradiating with circularly polarized light of R or L helicities respectively and simultaneously stirring mechanically the solution with ultrasonic waves. Figure 1.6 summarizes the findings [14]

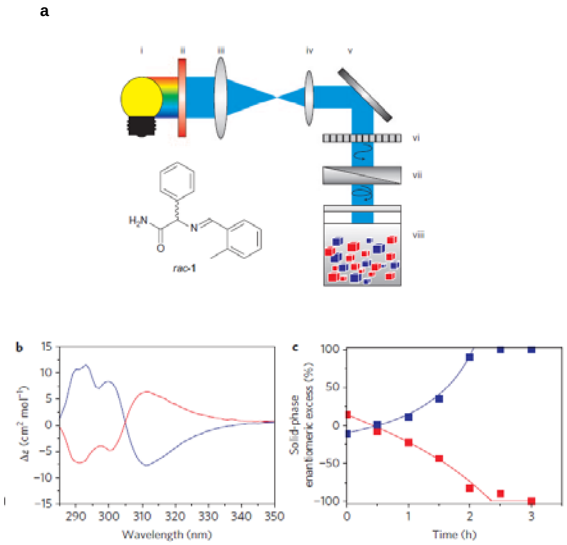

Figure 1.6 .

(a). Light from a 200W Xe discharge light source is focused and transformed to R or L circulary polarized. The light irradiates solutions or suspensions of a compound designed rac-1. (b) CD spectra of enantiopure solutions (c) temporal evolution of the enantiomeric excess with irradiation.

The 100% enrichment shown in the figure requires abrasive grinding of the solution. Glass beds were added to the solution that was installed in a standard ultrasonic cleaning vessel. The results illustrate the importance of diffusion processes in the solution and of aggregation on crystal faces in the chiral imbalance process, induced deterministically by the mechanical stirring. The microscopic origin of these processes is at present essentially unknown.

1.4 Experimental aspects .

Almost 100% of the operating CD setups are based on an optical scheme, developed more twenty years ago, that has proven to be extremely good and that it is appropriate to describe in this section.
Figure 1.7 shows schematically the components of a conventional CD instrument [15].

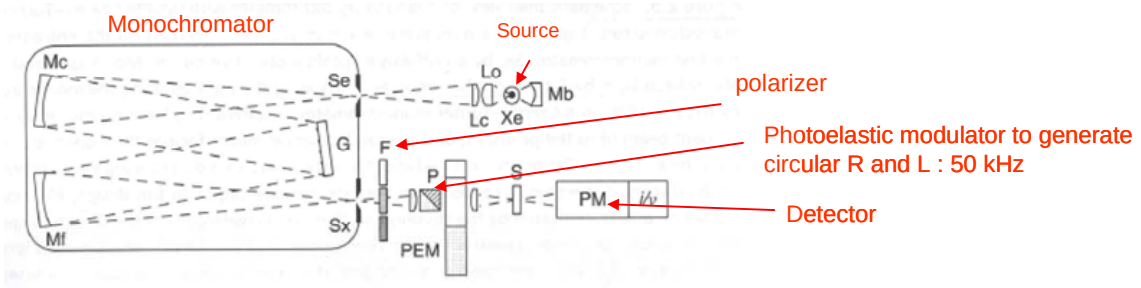

Figure 1.7.

Schematics of a conventional CD spectrometer.

The source is usually a 100-150 W Xe arc discharge lamp which generates photons in the visible and UV range. Typically a lamp produces at $\lambda = 200$ nm and $\Delta\lambda = 1$ nm about 10^{13} photons /s . The emitted photons are focused to the entrance slit and are collimated by the Mc mirror to impinge on a grating with variable incidence angle that acts as monochromator. The monochromatized flux is focused to the exit slit. A linear polarizer intercepts the beam and polarizes the light at 45 degrees from the vertical direction and a photoelastic modulator (PEM) polarized with a ac voltage generates R and L circularly polarized light. The PEM operates by generating a periodic strain produced by a piezoelectric transducer cemented to a fused quartz block or similar material which resonates longitudinally at a given modulation frequency. The periodically changing index of refraction in the quartz introduces a phase shift on the transmitted light that results in alternatively R and L circularly polarized light beams with a frequency equal to the excitation frequency [16]. Almost all the instruments of the world utilize PEMs modulated at 50 kHz. The transmitted light through the sample is collected by a fast detector, usually a photomultiplier. If the sample has circular dichroism then the periodically varying detector signal will have on top of a dc part an ac component at 50 kHz which amplitude will be proportional to the dichroism. [17] . The ac amplitude may be measured with a lock-in amplifier operating at the modulation frequency or by digital methods involving Fourier analysis.

A very important aspect of this measuring technique is the fact that as the dichroic signal oscillates at a frequency much higher than those generated by mechanical vibrations, electrical noise or other common sources of instabilities , the accuracy of the measured dichroism can very high reaching 10^{-5} in the best conditions. This remarkable fact has probably been the key for the success of this technique.

Perhaps the main limitation of the above experimental set up relies in the fact that as light has to be transmitted through different optical elements (polarizer, PEM…), the available wavelength range at the sample is determined by the combined optical transmission of the optical elements. In most conventional instruments synthetic quartz is the material of choice for the PEM . However, below 165 nm its transmission is very poor. Due to this, for operating in the VUV , CaF_2 or sometimes the less stable LiF are the best choices. Figure 1.8 shows the transmission of CaF2 for different wavelengths.

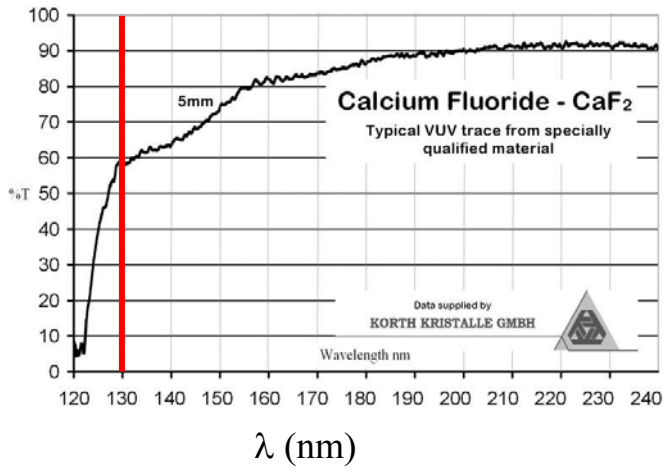

Figure 1.8.

Percentage of transmission of 5 mm of calcium fluoride. Below 130 nm (9.5 eV) the Transmission drops abruptly. The measured direct band gap of CaF2 is approximately 10 eV.

The most advanced laboratory instruments reach 160 nm as the lowest wavelength with acceptable intensity. The flux at the sample at 250 nm is typically in the 10^{10} ph/s range and decreases considerably below ~220 nm.

1.5 Synchrotron Radiation SRCD.

The first SR spectrometer operating above 100 nm designed for measuring ,among other, CD spectra was built at NSLS in 1980 [18] and the first SRCD spectra in the range 132-205 nm were collected at the Synchrotron Radiation Center of the University of Wisconsin-Madison [19] . They showed better signal to noise spectra that conventional laboratory equipments which allowed increased spectral resolution. The decade 1990-2000 led to a major growth of the technique. At present there are about 14 operating beamlines worldwide almost all installed in bending magnet sources as shown in the following table from [20] collected in 2010. In the years 2007-2010 for example, more than 4000 papers have included SRCD for the characterization of proteins.

Table 1. *Characteristics of SRCD Beamlines*

SRCD Beamline ID	U11	U9b	3.1	CD12	UV1	CD1	BL15	4B8
Synchrotron	NSLS	NSLS	SRS	SRS	ISA	ISA	HISOR	BSRF
Location	USA	USA	UK	UK	Denmark	Denmark	Japan	China
current status	operational	operational	closed	closed	operational	operational	operational	operational
added features	LD	SF,LD,F		SF	LD	LD		TJ,F
energy (Gev)	0·8	0·8	2·0	2·0	0·58	0·58	0·7	2·5
wavelength range	120–300	160–1500	130–350	100–700	130–450	115–350	140–310	120–350
max flux@ 240 nm (ph/s)	3·00E+12	9·00E+12	3·00E+10	2·50E+13	1·50E+11	1·00E+12	2·00E+10	8·00E+10
max flux@ 180 nm	2·50E+12	2·00E+12	4·00E+10	2·50E+13	1·50E+11	1·00E+12	8·00E+10	2·00E+11

SRCD Beamline ID	3m_NIM-C	04B1	BL-5B	B23	DISCO	CD12	U25	
Synchrotron	BESSY2	NSRRC	TERAS	Diamond	Soleil	ANKA	NSRL	AS
Location	Germany	Taiwan	Japan	UK	France	Germany	China	Australia
current status	operational	operational	operational	commission	commission	develop	develop	planning
added features	CF	SF(p)	LD	SF(p)	SF(p)			
energy (Gev)	1·9	1·5	0·3–0·8	3·0	2·75	2·5	0·8	3·0
wavelength range	130–300	130–330	70–250	120–300	120–600	120–350		
max flux@ 240 nm (ph/s)	2·00E+11	1·00E+11					1·50E+12	
max flux@ 180 nm	5·00E+10	1·00E+11					2·00E+12	

(Some minor corrections to the table are: B23 [21] and DISCO [22] are operational. The lowest wavelength range of the beamline at TERAS is most likely 170 nm and not 70 nm although it has not been possible to confirm it) .

As visible in the table the maximum flux at 240 nm ranges from 10^{11} to 10^{12} ph/s at the sample including B23 [21] and DISCO [22] , and the available wavelength range is typically 120-300 nm approximately.

All the beamlines in the table operate with the same basic optical scheme than in commercial instruments i.e. all of them utilize PEMs to generate circular light from the plane polarized radiation generated at the bending magnet source. In most cases, the PEMs are made of CaF_2 crystals, and attenuators are sometimes needed to avoid damaging the PEM if illuminated with intense beams [21,23]. In almost all cases there are UV transmitting windows separating the sample area and the optics.

A special and unique beamline that is not included in the above table and that allows CD measurements (and other spectroscopies) using an undulator source instead of a bending magnet is DESIRS [24] at Soleil. We will discuss it in section 2.3.

Generally speaking, the available photon flux generated at synchrotrons is about 2-3 orders of magnitude higher than laboratory instruments allowing to extend the usable wavelength range to short wavelengths even with low transmitting optical elements as illustrated in Figure 1.9 from ref [25] .

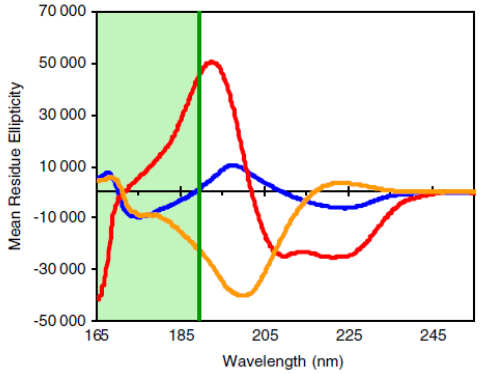

Figure 1.9.

Comparison of the wavelength ranges of conventional CD and SRCD spectra of several proteins. SRCD allows to probe the green area in addition to the white area measured in conventional laboratory CD instruments .

To illustrate the possibilities of synchrotron radiation CD spectroscopy, we reproduce results of a pioneer work of D.T. Clarke et al. [26] done at the Daresbury Laboratory Synchrotron Radiation Source. The authors investigated the kinetics of α– helix folding with time resolved CD spectroscopy with an acquisition time of 2.5 ms per spectrum in the range 190nm -242 nm

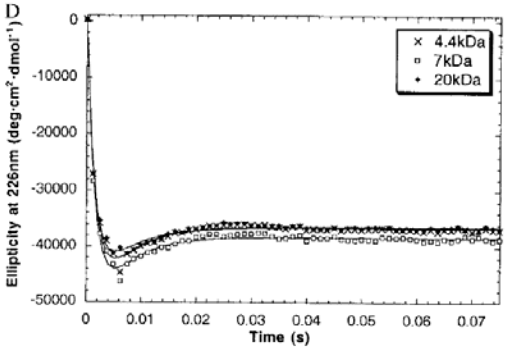

Figure 8.

Temporal evolution of the ellipticity at 226 nm revealing the kinetics of the α helix folding rate. A fast initial decay till 5 ms is followed by a slower kinetics

2.- Motivation of Skiron. Branch A

2.1 Deep molecular orbitals

An important example of application of electronic CD that has been extensively investigated is the amide group within macromolecules . Figure 2.1 depicts its electronic orbitals in the UV region.

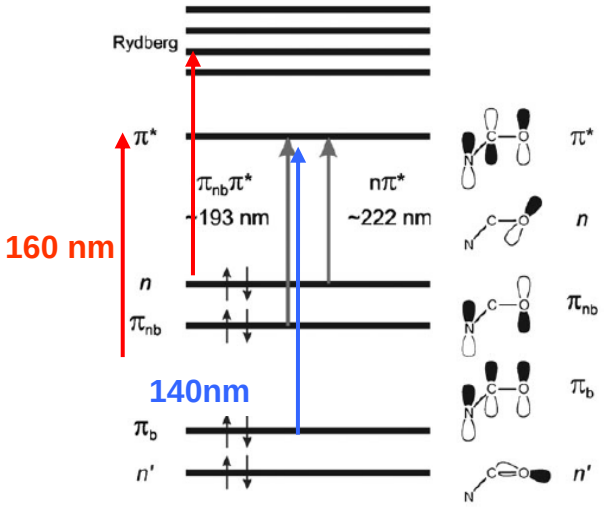

Figure 2.1.

Electronic structure of the amide group showing the topmost molecular orbitals and several electronic transitions (see text).

In a α-helix , for example, the CD shows a positive band at ~193 nm and a negative one at 208 nm arising from the exciton splitting of the electronic transitions π_{nb} to π* as depicted in the figure with a black arrow [27]. Also, a negative band at ~222 nm originates from a non bonding oxygen orbital , n, to π* as indicated. The red arrows correspond to 160 nm wavelength which is in many practical cases the shortest available. As seen, the π_b and n' transitions to the antibonding π* cannot be excited. In addition, the series of Rydberg states schematically shown in the figure, which converges to the ionization potential, are only partially reachable from the n orbital.

Although the available experimental data are scarce, several publications stress the interest for searching high energetic molecular transitions. J. Jianj et al. [30] report measurements and calculations down to 165 nm of protein backbone transitions displaying relatively large signals at the lowest wavelength. K. Gekko et al. [31] using a specially designed synchrotron radiation CD (SRCD) system, report non zero intensities down to 140 nm and distinct signals at ~170 nm from L-Isomers of aminoacids which are attributed to electronic transitions of the carboxyl groups. Clayton et al. [32] show measurements from nicotine in the range 180-300 nm that exhibit the most intense CD signals at the lowest measured wavelength. From the theory side, Serrano et al. [33] investigate the electronic structure of peptides and show that in addition to the well-known transitions at 220 and 190 nm, polypeptides have bands at 165 –170 nm which later have been brought to experimental evidence. An earlier calculation by Clark [34] reports absorption bands from carboxyl groups at 156 nm and from amide groups at 128 and 139 nm.

As a matter of fact, deep molecular orbitals provide additional opportunities for spectroscopy as it will be shown next.
Figure 2.2 (left) shows data from the gas phase photoemission beamline at Elettra [28].

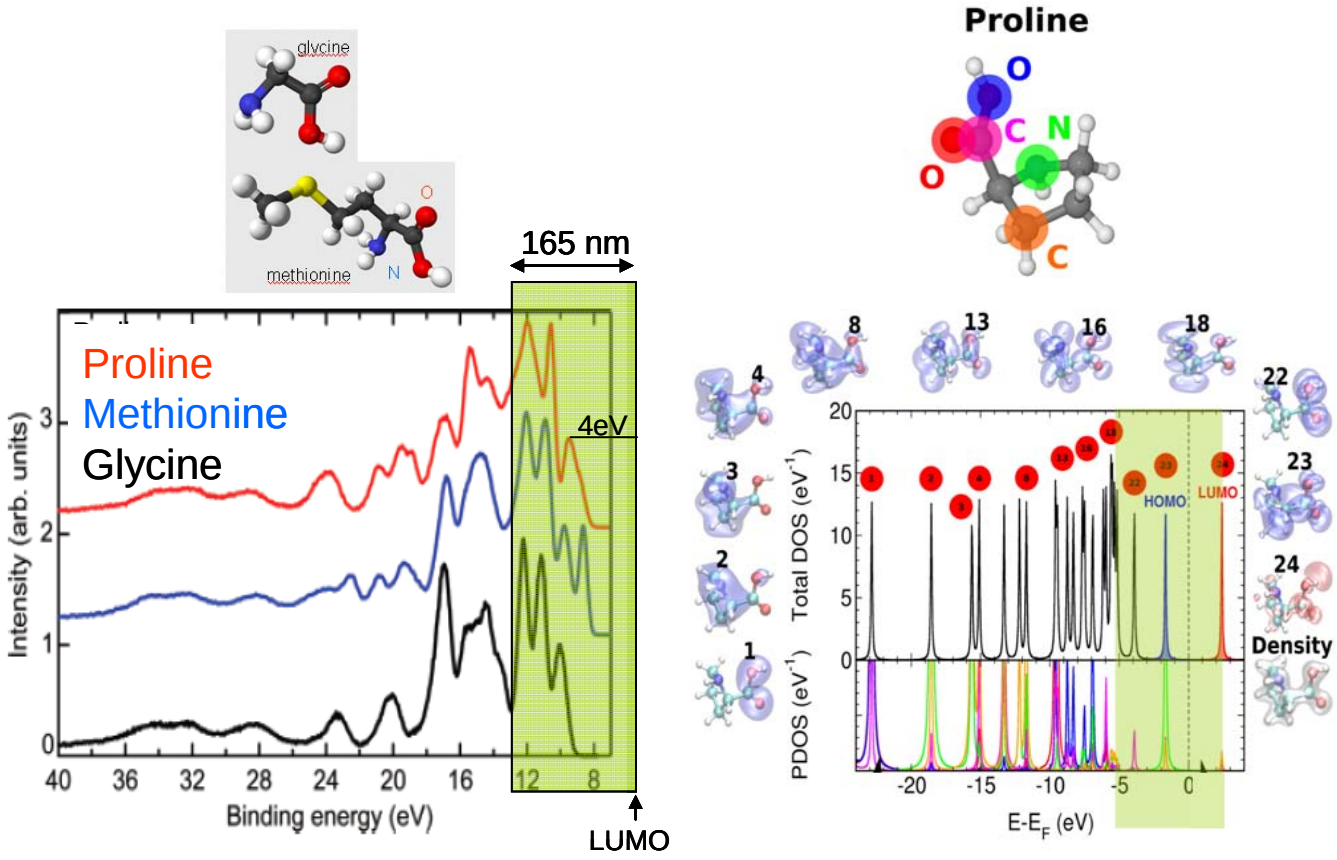

Figure 2.2.
Left panel : Gas phase photoemission from simple aminoacids with their molecular structures.
Right : Calculated partial and total density of states of proline. [29]

The measurements were done at hν = 99 eV using a crucible to heat the aminoacids in order to achieve significant vapor pressures in the 10^{-5} mbar range .
The shaded rectangle has a width of 7.5 eV (165 nm) and it has been located with the right end side at 4 eV from the HOMO (Highest Occupied Molecular Orbital) orbital of proline which is roughly the location of the LUMO (Lowest Unocuppied Molecular Orbital). Only transitions with initial state in the shaded area, having the LUMO orbital as final state, are accessible with $\lambda \geq 165$ nm. As seen in the figure, the binding energies

of the HOMO orbitals are around 9-10 eV and consequently it is not possible to excite transitions from the occupied orbitals to the continuum with photons with $\lambda \geq 165$ nm. The right panel is a calculation of the partial and total density of states for the proline gas phase molecule [29]. The shaded area shows again the possible transitions from filled states to the LUMO for $\lambda \geq 165$ nm. Only the transitions with the initial states labeled 18, 22 and 24 are energetically possible. The figure also shows the spatial distribution of the electronic density for several states.

The above two examples illustrate that increased photon energies would allow to excite additional electronic transitions that might be optically active and provide additional spectroscopic information. That comprises transitions from deep molecular orbitals to the LUMO or transitions from occupied orbitals to the continuum . In the first case the transition is associated to absorption of photons whereas in the second one, in addition, photoelectrons are generated as a consequence of the absorption .

Photoemission from deep molecular orbitals coupled to the variable photon energy from synchrotron sources, opens the opportunity of investigating resonant photoemission processes.

Figure 2.3 from ref. 96 depicts the concept and experimental results from Mn atoms in the vapor phase.

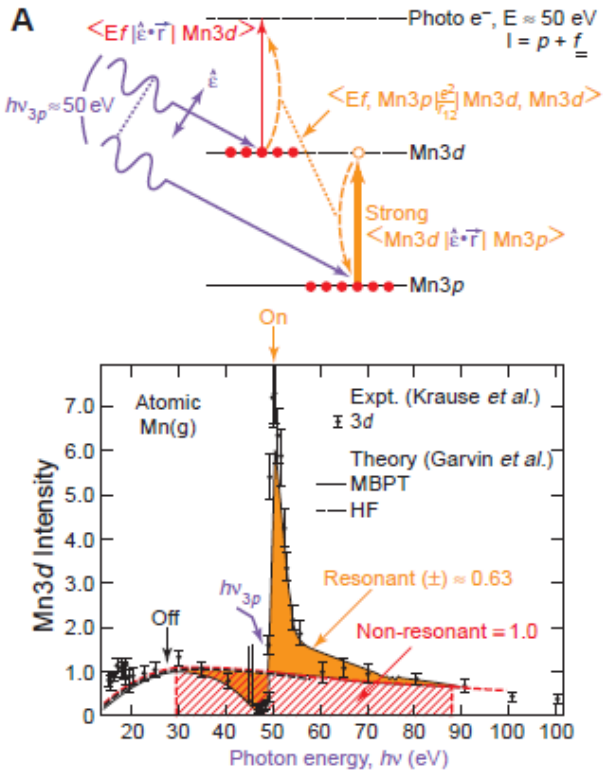

Figure 2.3

Top:
Schematics of the resonant process due to the interaction of the two optical transitions. The strong dipolar transition 3p-3d couples to the photoemission channel 3d-continuum.

Bottom:
Photoemission intensity from 3d to the continuum vs photon energy. The colored orange region indicates the resonant part of the intensity.

Suppose a photon of energy equal to that required to excite a 3p electron to the 3d shell as indicated with the orange arrow in the figure. The relaxation of the excited electron to its initial state is a fast process that couples to the photoemission of a 3d electron to the continuum indicated with the red arrow. Both processes (orange and red arrows) may be considered simultaneous and coherent and result in an enhanced photoemission yield. The orange shaded part of the experimental data indicates the resonant process. At the resonant energy the intensity of the 3d photoelectron peak is about 7 times larger than below the resonance.

Resonant photoemission in biomolecules might produce interesting results as illustrated below.

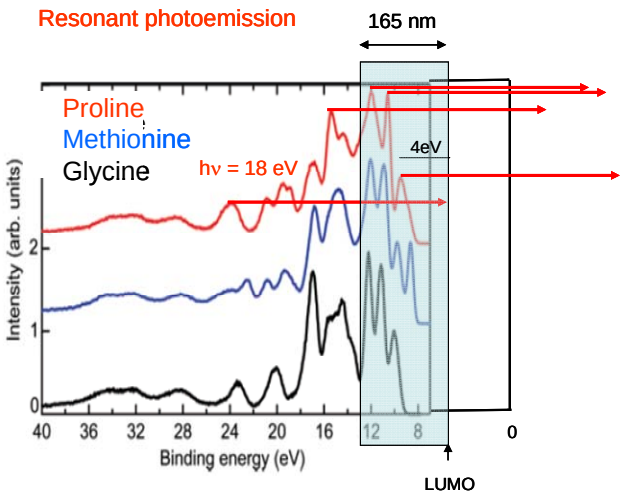

Figure 2.4

Examples of possible resonant photoemission at hν = 18 eV in proline molecules.

The red arrows of the figure correspond to photons with the precise energy to excite electrons from the molecular orbital of proline at 24 eV to the LUMO (hν ~ 18 eV). As it may be seen, several resonant process from the upper molecular orbitals to the continuum are in principle possible and might result in increased photoemission yields and perhaps in distinct optical activity.

The resonant photoemission process may involve different atoms of the same or different chemical species. As shown in figure 2.3 the resonance may be viewed as a result of the interaction of the two excitons generated by the absorption of two photons. In this sense , it reminds the excitonic model mentioned in 1.2 which produces an energy level splitting where each level has a different sign of the rotary power. As a consequence , variation of the photon energy produces positive and negative CD as, for example, in figure1.4 panel c. One may speculate if similar phenomena would occur in resonant photoemission. Referring to the bottom panel of figure 2.3, it might occur that the negative low energy side has CD of opposite sign than that of the positive high energy side.

Summarizing, we consider that the above arguments and examples provide a basis to expect that interesting scientific results may emerge from exploring the optical activity of deep molecular orbitals which is the main motivation of the branch A of Skiron.

However, to explore optical transitions below 165 nm, it is required that the photons reach the molecules of interest.
In the very important case of molecules in aqueous solution, one faces with a "hard wall" given by the optical transmission of liquid water which is displayed in figure 2.5.

2.2 The opacity of water below ~180 nm

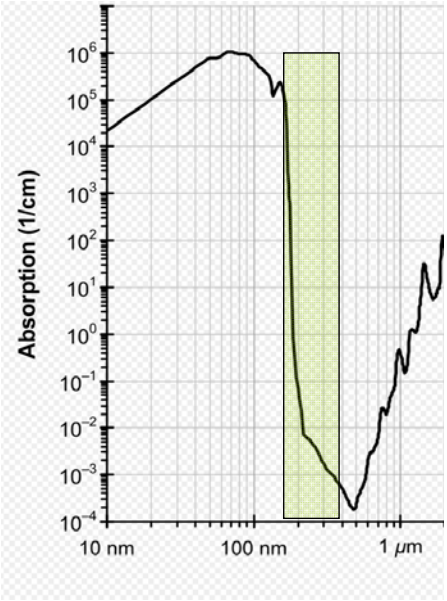

Figure 2.5

Optical absorption of liquid water. The rectangular green area denotes the wavelength range available from existing laboratory instruments and beamlines. At λ= 160 nm the 1/e attenuation length is ~10^2 μm and at λ = 140 nm is ~0.05 μm . There is a "hard wall" in transmission for $\lambda \leq$ 150 nm approximately .

The opacity of water in the far UV leads to two scenarios to access the CD of relevant molecules: gas phase photoemission experiments or photoemission from solutions in liquid jets.

2.3 Gas phase photoemission and CD

As already mentioned in 1.2, evidence for CD in gas phase molecules was demonstrated in 2001 using the asymmetric photoemission effect. Since then, several groups have further developed this research area particularly Nahon et al. [24] at DESIRS (Soleil)

[and Turchini et al. at the CiPo beamline at Elettra [35] . An example from Elettra that illustrates the possibilities of the technique is given below.

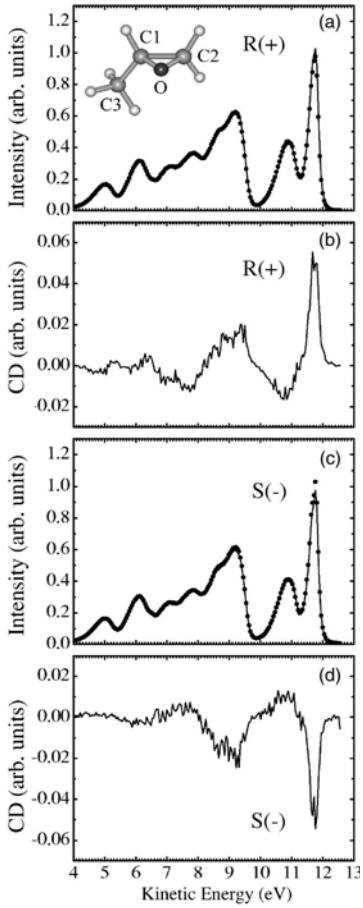

Figure 2.6

Representative results form gas phase dichroism measurements from in methyl-oxirane.
The authors investigated both enantiomers of the chiral molecule (R and S) by using photons of 22.0 eV . Panels a and c are photoelectron spectra for R and S molecules measured with right (solid line) or left (dots) handed circularly polarized light. The inset shows the structure of the C3H6O molecule . Panels b and d are the dichroic ($I_+ - I_-$)/($I_+ + I_-$) spectra for R and S methyl-oxirane.

The spectra were acquired by flipping the helicity of the radiation generated by an helical undulator at a frequency in the range 0.1-0.05 Hz.
The gas sample was introduced with a needle which generated an effusive jet beam at room temperature.
The experimentally determined D values are different for different initial states ranging from -0.02 to 0.05. From ref. 36

If instead of effusive gas sources generating a Maxwellian velocity distribution with temperatures around 300 K , one uses supersonic jets of gas obtained from adiabatic expansion of a high pressure gas through a nozzle/skimmer combination [37] , then the experimental possibilities broaden considerably since as the gas temperatures are of few tens of K, it may occur that the lowest energy conformer becomes the most abundant since thermal excitation may not be enough to overcome the barriers with other higher energy conformers.
Gas phase CD measurements of adenine, cytosine and alanine [38], [39] nicely illustrate the possibilities of the asymmetric photoemission technique in fundamentally important biomolecules.

Whereas supersonic cooled jets of gas at synchrotron facilities are presently used only at DESIRS, laser spectroscopists have use them for several years . For example, Al-Rabaa and coworkers [40] employed laser-induced fluorescence techniques to discriminate between pairs of weakly bound species. By using 2-naphthyl-1-ethanol (2-NetOH) as the chiral chromophore they investigated the effect of complexations with different alcohols either chiral or achiral. The resulting homochiral or heterochiral pairs were identified

with fluorescence spectroscopy and analysis of the data and theoretical considerations allowed to conclude that the geometrical structure of the homochiral pairs is extended while that of the heterochiral is folded.

Speranza and coworkers published a recent review of their extensive work [41] describing the progress of gas phase recognition of chiral systems of biological interest using the mass resolved Resonant Two Photon Ionization (R2PI-TOF) technique in supersonic beams. The measurement of absorption spectra, ionization and fragmentation thresholds of diastereomeric clusters by this technique allows the determination of the nature of the intrinsic interactions, which control their formation and which affect their stability and reactivity. The basic motivation was to obtain information on chiral recognition and rate acceleration in biological processes. This was achieved by preparing aggregates of the same or different handeness associating for example a right handed chromophore to a right or left handed chiral solvent molecule and investigating their spectroscopic signatures.

It is likely that in the next years the above research on combinations of molecules with the same or different chirality will be undertaken at synchrotron facilities to achieve complementary inputs to these interesting phenomena.

2.4. CD Photoemission from liquid jets

To extract the optical activity of molecules in solution at photon energies above the water "hard wall " at ~7 eV an interesting possibility is to use the asymmetric photoemission from liquid jets of the solutions of interest.

Photoemission from liquid jets is a well established technique developed by Faubel and coworkers in the last decade [42-45]. At present is being used at Bessy, ALS and more recently at MAX lab. Most of the published work deals with core level photoemission from C1s, O1s, K 2p, I 4d being the work from the valence emission less common. Figure 2.7 shows the operating principle.

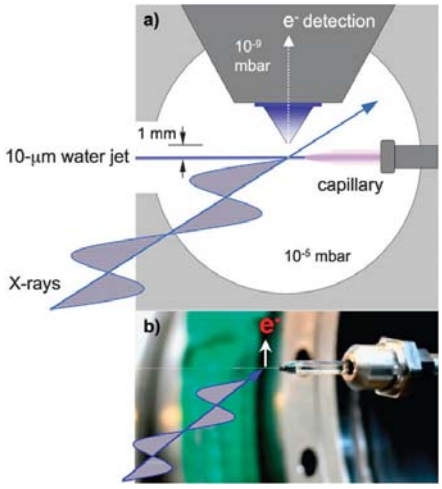

Figure 2.7

Schematics of the liquid jet system. The liquid jets are formed by establishing a pressure of 5-20 bar of liquid in the back side of a 10-15 μm diameter nozzle situated at ~2mm from the photon beam direction and at ~1 mm from the entrance nozzle of an electron energy analyzer with one stage of differential pumping. (from ref. 45)

An interesting aspect is the following. As the collected photoelectrons will generally have small kinetic energies, their mean free path for inelastic scattering will be larger that for photoelectrons of a few hundreds eV due to the shape of the so called "universal curve"

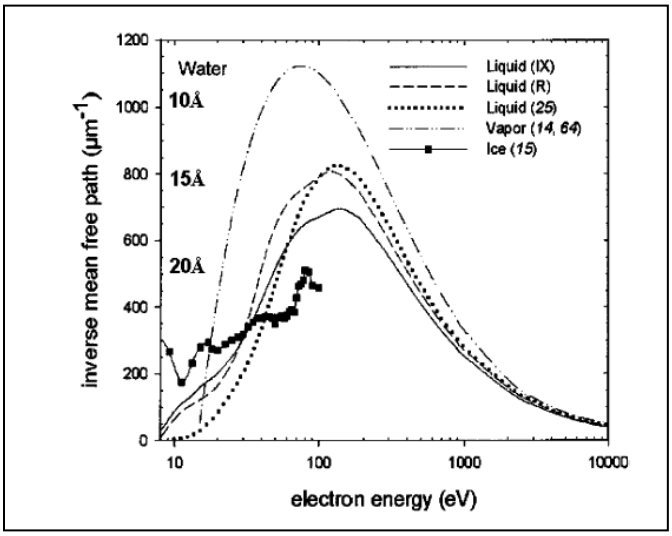

Figure 2.8

Inelastic inverse mean free path of electrons in water calculated using different models. The data points are experimental values from amorphous ice. At the right side of the ordinate axis the mean free paths are indicated. As it may be seen, at 10 eV kinetic energy the value is 250 μm $^{-1}$ i.e. a mean free path of about 40 Å. (from reference 42)

An example of valence band photoemission is depicted in Figure 2.9 from [42]

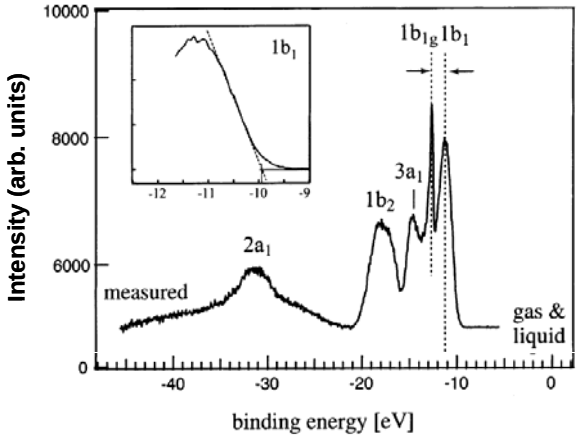

Figure 2.9.

Valence band photoemission from liquid water (hν = 60 eV). The molecular orbitals are indicated. The sharp peak $1b_{1g}$ arises from vapor at the vicinity of the liquid jet. The zero binding energy refers to the vacuum level.

In summary, at branch A we envisage to perform CD spectroscopy in a wider energy range than that of the beamlines in table I . Skiron will provide photons with energies high enough to explore electronic transitions involving deep molecular orbitals, by means of asymmetric photoemission spectroscopy, of molecules in the gas phase from effusion gas cells and from solutions in liquid jets.

3.- Motivation of Skiron : Branch B

3.1 CD measurement in anisotropic media

In an isotropic optically active solution any incoming left- or right- circular polarized light will keep its circular polarization, and only the intensity will be affected. On the contrary, in an anisotropic medium the circular polarization is no longer preserved and the emerging light beam will be in general elliptically polarized. Conventional instruments and method to CD cannot follow this change of type of polarization and, therefore, they do not offer reliable measurements whenever there exists anisotropy (i.e. some type of preferential orientation) in a medium [46-49]. In terms of an optical measurement the anisotropy results in linear birefringence and linear dichroism. In practice, most solutions involving small molecules or gas phase samples do not show difficulties for the assessment of chirality due to the absence of linear dichroism and linear birefringence. This is the case of solutions of spherically shaped colloidal particles as those of globular proteins. Their isotropic statistical distribution cancels any eventual linear anisotropy. However, this is not the case of systems containing macromolecules [50,51], for example fibrous proteins or aggregates, or in any CD measurement performed in the solid state.
The determination of CD in anisotropic systems becomes less straightforward than in the isotropic case, and it is necessary to consider how the linear anisotropies may combine to produce a differential absorption of circularly polarized light (CPL) that can be confused with CD. To properly measure optical activity in oriented systems it is necessary to generalize what it is usually referred as a *CD measurement* to *a Mueller matrix measurement*. The 4×4 Mueller matrix ($\mathbf{M} \mid M_{ij} \in \mathbb{R}$) is a linear operator that completely describes the linear optical response of a material for any form of incoming polarization [52,53]. A Mueller matrix **M**, which is parameterized as

$$\mathbf{M} = \begin{bmatrix} M_{00} & M_{01} & M_{02} & M_{03} \\ M_{10} & M_{11} & M_{12} & M_{13} \\ M_{20} & M_{21} & M_{22} & M_{23} \\ M_{30} & M_{31} & M_{32} & M_{33} \end{bmatrix},$$

transforms the polarization state of the input light expressed as a Stokes vector (***S***) whose components are sums and differences of the intensities of various polarization states (linear polarization states: I_x, I_y, $I_{\pm 45}$; circular polarization states: I_R, I_L) into output light with a polarization state defined as some other Stokes vector, $\mathbf{S_{out}} = \mathbf{MS_{in}}$. Polarimeters are optical instruments that serve to measure one or more elements in **M**. For instance, most CD spectropolarimeters intended for the analysis of isotropic solutions deliver M_{03} by modulating the input light polarization with a single photoelastic modulator. Under the suitable conditions of isotropy, M_{03} can be taken to equal *CD,* however, in the most general case a physical interpretation of the elements in **M** requires the complete knowledge of the matrix.

For nondepolarizing media, the Mueller matrix has at most seven parameters [46,54], that are introduced in Table 1. A general nondepolarizing Mueller matrix can be constructred from its infinitesimal generator **L**, known as the differential Mueller matrix [55,56]:

$$\mathbf{M} = \exp \mathbf{L}, \text{ with } \mathbf{L} = \begin{bmatrix} A & -LD & -LD' & CD \\ -LD & A & CB & LB' \\ -LD' & -CB & A & -LB \\ CD & -LB' & LB & A \end{bmatrix},$$

where *exp* is understood as matrix exponential, and the isotropic absorption (*A*) acts as a uniform scaling. In transmission, the entries in **L** have a direct physical interpretation as the fundamental optical properties (*LD*: linear dichroism, *LB*: linear birefringence, and unprimed or primed terms refer respectively to a set of axis at 0, 90 deg or 45, 135 deg; *CD* = circular dichroism; *CB*: circular birefringence). With knowledge of **M**, Eq. 1 can be inverted numerically by taking the logarithm of **M** or with an analytical method recently described [57]. In the case of depolarization, the symmetry of **L** may be broken, and the optical properties are then taken as the average values of related elements [58, 59] (e. g. $CD = \frac{1}{2}(L_{03} + L_{30})$, $CB = \frac{1}{2}(L_{12} - L_{21})$) however, for most of the samples of interest in chemistry and biology the depolarization is almost negligible and Eq. 1 is valid.

Effect	Symbol	Definition[a]
Isotropic amplitude absorption	*A*	$2\pi\kappa l/\lambda_0$
(*x*–*y*) linear dichroism	LD	$2\pi(\kappa_x-\kappa_y)l/\lambda_0$
(*x*–*y*) linear birefringence	LB	$2\pi(n_x-n_y)l/\lambda_0$
45° linear dichroism	LD’	$2\pi(\kappa_{45}-\kappa_{135})l/\lambda_0$
45° linear birefringence	LB’	$2\pi(n_{45}-n_{135})l/\lambda_0$
Circular dichroism	CD	$2\pi(\kappa_- - \kappa_+)l/\lambda_0$
Circular birefringence	CB	$2\pi(n_- - n_+)l/\lambda_0$

[a], n is the refractive index; κ, extinction coefficient; l, path length through the medium; λ_0 vacuum wavelength of light. Subscripts specify the polarization of light as x, y, 45° to the x axis, 135° to the x axis, circular right +, or left −.

Table 3.1. List of the seven properties that describe the interaction of a medium with polarized light.

Under the common approximation of small optical properties (all optical properties < ~ 0.5 rad) **M** is well approximated by keeping up to second order terms in the Taylor series expansion of exp(**L**) [60] giving:

$$\mathbf{M} \approx \mathbf{L} + \frac{1}{2}\mathbf{C}^2$$

$$\mathbf{C}^2 = \begin{bmatrix} CD^2 + LD^2 + LD'^2 & -CDLB' + CBLD' & CDLB - CBLD & -LDLB' + LBLD' \\ CDLB' - CBLD' & -CB^2 + LD^2 - LB'^2 & LBLB' + LDLD' & -CBLB - CDLD \\ -CDLB + CBLD & LBLB' + LDLD' & -CB^2 - LB^2 + LD'^2 & -CBLB' - CDLD' \\ LDLB' - LBLD' & -CBLB - CDLD & -CBLB' - CDLD' & CD^2 - LB^2 - LB'^2 \end{bmatrix}$$

The entries in $\mathbf{C}^2$ represent additional contributions to **M** from the mixing of the optical properties. This analysis is only approximates, but it gives an idea of how the optical properties mix in **M**. We see that the common assumption of $M_{03} = M_{30} = CD$ is only valid when the factor $LBLD' - LB'LD$ vanishes.

To understand under which conditions the extra term vanishes, it is convenient to express *LD* and *LD'*, the two different projections of linear dichroism, as $LD = \|LD_\chi\| \cos 2\chi$ and $LD' = \|LD_\chi\| \sin 2\chi$, in which $\|LD_\chi\| = \sqrt{LD'^2 + LD^2}$ is the total linear dichroism and χ is the angle between the dichroic axis and the instrument *x* axis. In the same way, we define the total linear birefringence LB_ψ where ψ defines the reference axis for birefringence. We can now express the extra term in M_{03} as,

$$C_{03}^2 = LBLD' - LB'LD = -\|LD_\chi\|\|LB_\psi\| \sin 2(\chi - \psi),$$

which is nonzero whenever the absorption and extinction axes are not parallel or perpendicular.

CD and CB, the optical effects linked to optical activity, are typically very weak, much smaller that LD and LB and therefore the contribution of these *artifact* terms can become much larger that the real CD and CB. Moreover, it is worth to recall that, very often, optical elements included the path of the beam (cuvette walls, optical windows, etc) show non negligible contributions of linear birefringence that when coupled with the linear dichroism of the sample can give rise to large combined effects that would be erroneously taken as CD, unless the whole Mueller matrix was measured.

One important field where these artifact terms play a very relevant role is in the study of proteins [61, 62]. Proteins are classified by their structural characteristics to be either globular, membrane bound, or fibrous. Globular proteins are usually highly aqueous soluble whereas membrane proteins are lipid soluble. They provide the majority of the enzymatic, regulatory, and signaling machinery required to maintain a cell. Fibrous proteins and proteins bound to membranes may show a preferred alignment in the solution (by effect of aggregation, weak convention flows, very short path length cuvettes, etc.) and be anisotropic due to the effect of order in the case of solid films. This leads to linear polarizations, which in principle might be interesting for structural differentiation (as it is commented in the next section) but, in practice, are an obstacle since as in most samples the orientation of the chromophore is unknown, linear polarization effects produce artifact CD signals. Therefore, the conventional circular dichroic spectra in such complex but common samples, does not correspond to the true CD spectrum and consequently the computer-based correlation methods between CD and structure [secondary structure (α-helix, type of β-sheets, etc) and tertiary structure changes] in protein clusters [63,64] might be inaccurate . This problem is even more important in the case of films of solid samples as are fibrous proteins, amyloids and prions. As an example, the recently reported [57] CD spectra of some natural amino acids in the wavelength range 140 nm–300 nm, required the preparation of amorphous, i.e. isotropically distributed, solid samples.

Researchers have been concerned about the study of chirality in anisotropic systems for decades, for example, Kuroda and coworkers have developed spectroscopic polarimeters for application to anisotropic materials in order to avoid artifact CD signals. These are the progressively more sophisticated so-called Universal Chiroptical Spectrometers (UCS) [58,59]. In these instruments, two lock-in amplifiers are used to monitor two frequencies derived from the PEM modulation, one at 50 kHz, and another at 100 kHz (2?). Because

only two frequencies are utilized in the analysis, some approximations are required to simplify the intensity expressions. It is assumed that the fundamental optical constituents that enter into the Mueller matrix are separable and that a variety of terms can be assumed to be small enough to be neglected. Only complete polarimetry, i.e. Mueller matrix polarimetry, is fully robust for the assessment of chirality in general anisotropic media.

Skiron will feature a transmission branch flexible spectroscopic Mueller matrix polarimeter, covering a spectral range from 130 nm to 400 nm. CD synchrotron beamlines all over the world use one photoelastic modulator (PEMs) to achieve a fast modulation of the polarization of beam [60]. Skiron will use 4-PEMs in the optical path instead of only one, this is to have access to virtually any state of polarization of light and, therefore, measure the complete Mueller matrix measurement (more details are given in the optical design section). Thanks to this general polarimetric approach Skiron will benefit of an unprecedented flexibility for the determination of optical activity, as it will be able to study isotropic and anisotropic systems, either in solution, gas or solid state.

Another field of application of a synchrotron Mueller polarimeter is the study of the optical properties of crystal structures and solid matter. These include VUV measurements of birefringence that are inaccessible using laboratory sources. For example, the birefringence of the CaF_2 lenses used for 157 nm optical lithography distorts de focal point of the laser light and needs to be carefully measured [65]. It will also serve to study the electronic band structure of optically anisotropic materials (ZnS, CdSe, rutile, etc) at photon energies above the bandgap if sufficiently thin specimens are analyzed or a reflection configuration is adopted [58]. If a magnet is introduced in the sample chamber Faraday rotation, magnetic circular dichroism are readily obtained from the Mueller matrix and they are useful to measure oscillator strengths [66]. Similarly, if an electrical field is applied to the material several electroptic effects (Pockels, Kerr, electrogyration, etc) are measurable [67]. In the field of liquid crystal electroptic effects are also crucial, but there are no studies with VUV radiation [68].

The 4-PEM Mueller matrix polarimeter has been recently implemented in a laboratory environment [69] with highly successful results, so many of detection routines and analysis procedures will be transferred to the synchrotron version of the instrument. Thus, all this preliminary experience offers the certitude that in relatively short time period, world-class polarimetric measurements with synchrotron radiation could be achieved. The next two sections highlight two other unique benefits that will offer the synchrotron 4-PEM polarimeter, with respect to the common CD spectroscopy systems available in other in synchrotrons: true LD spectroscopy and space resolved (mapping) measurements.

3.2 Linear Dichroism spectroscopy. Importance and applications

In addition to CD spectroscopy, the Mueller matrix approach for chiral assessment provides, at the same time that CD is measured, a full characterization (magnitude and orientation) of linear dichroism (LD). Since only oriented molecules show different absorbance for different polarizations, LD detects only oriented molecules. This means it is possible to study one molecule against a background of many absorbing species--as long as the molecule we are interested in can be oriented. There exist many methods to orient molecules, for example in aqueous solutions, flow orientation is an attractive orientation methodology as it selects longs molecules or molecular assemblies (or ones that can be induced to adopt a high aspect ratios by the flow, such as liposomes). If we measure the absorbance of light by flow-oriented molecules then we get the same spectrum as for a non-flowing solution unless the light we use is linearly polarized. LD thus is selective for molecules that are particularly challenging to study by more standard biophysical techniques

LD spectroscopy has been applied to study the functionality and structure of a large number of systems involving macromolecules [70-72] , for example DNA, DNA--drug systems, DNA--protein enzymatic complexes, fibrous proteins, such as those involved in Alzheimer's disease, and membrane peptides. Knowing the structure of a molecule is one of the keys to deducing its function in a biological system. Many biomacromolecules, however, are not amenable to structural characterization by powerful techniques such as NMR and X-ray diffraction because they are too large, too flexible or cannot be crystallized. All these long molecules are best studied in the UV or VUV, so Skiron can provide the perfect range of energies for these measurements. For example, the DNA molecule is very long and very thin, making it very easy to orient in flow. This gives rise to a strong LD signal as it is shown in Fig. 1. DNA systems that have been studied using UV LD include DNA-enzyme complexes and DNA-ligand complexes

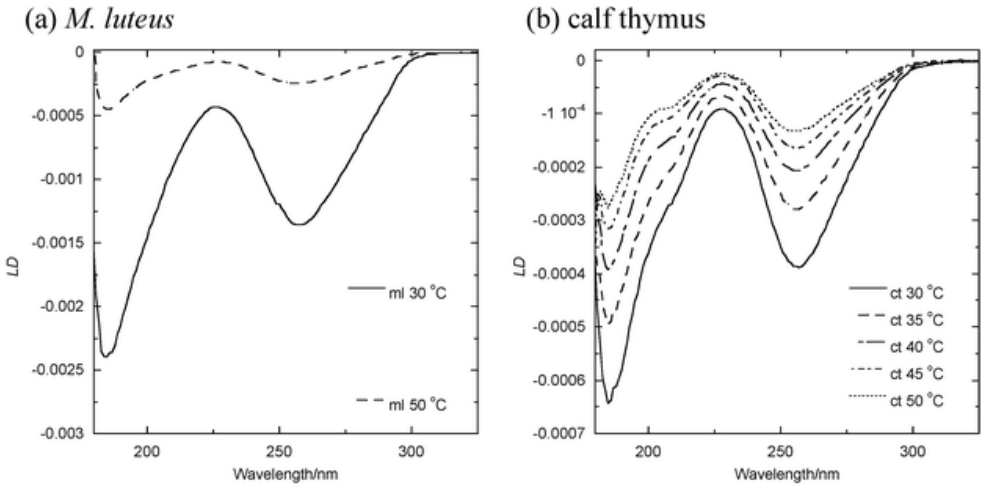

Fig. 3.1 LD spectra of different DNA in water at different temperatures. Measurement made with Couette flow cell spinning at ~3000 rpm. Adapted from Ref. [28].

LD spectroscopy obtained from a Mueller matrix experiment has advantages over conventional LD spectroscopy, since it provides the magnitude of LD (that gives insight into the chemical structure of the molecule) but also the orientation of the molecule [47]. In conventional systems, the experimentalist has to know with anticipation the orientation of the molecules in the flow and only then he can measure the magnitude of LD. Therefore, the alignment methods used to orient the molecules can be very flexible, as any orientation of the plane is valid for measurement. Which orientation method one should be use for LD depends on the type of sample. Long and relatively rigid polymers, such as double-stranded DNA or RNA, fibrous proteins or molecular assemblies of micrometer dimension, may be oriented by shear flow whereas small molecules require a stronger orienting force. Some molecules which cannot themselves be oriented may orient when they bind to another molecule that is already oriented.

If a rigid or semi-flexible polymer, such as DNA, is dissolved in a solvent then flowed (laminar flow), then the molecules experience sufficient shear forces to give a net orientation of the long axis of the polymer along the flow direction. This physical effect is exploited in the famous Couette flow cell (Fig. 2) in which the molecules are oriented by the viscous drag caused when a solution is flowed between the annular gap of a cylindrical cuvette with a rotating quartz rod in the middle. This technique is commonly used for LD studies of DNA. The advantage of the Couette cell over a flow-through system is that the same volume of sample can be measured indefinitely. Improved cell designs have reduced the amount of sample required to as little as 30 μL, making the technique valuable even on a biochemical volume scale.

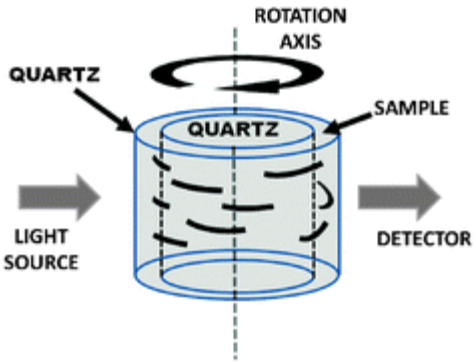

Fig 3.2. Scheme of a Couette cell

The interpretation of LD spectra is challenging, since overlapping transitions lead to the cancellation of bands and complicate the analysis of experimental spectra. However, quantum-mechanical calculations (similar to those made for CD) allow one to study both single and multiple transitions as a function of geometry and orientation. Therefore the comparison between LD experiments and calculations can lead to mechanistic and structural details of the molecules. The differences between LD and CD spectroscopies are complementary and can be a powerful means for elucidating the structure of biological molecules when used in conjunction with one another, the combination of techniques revealing far more information can a single technique in isolation. For example CD tells us when a membrane peptide or protein folds whereas LD tells when it inserts into a membrane [74].

3.3 High Spatial resolution through Mueller matrix imaging or microscopy.

The optical properties of a medium can be very inhomogeneous. This is typical for solid state samples, but it can also apply to liquid samples subjected to flows. In these situations, the optical properties of a medium can vary a lot from point to point and a reliable measurement is only possible if there exist some degree of spatial resolution. In the limiting case, it can be necessary to have a micrometric resolution to isolate the sample or portion of medium of interest from the background. For example, one of the most complicate systems to study that one could imagine is the optical activity of an anisotropic microcrystal, a problem which only recently has been investigated in laboratory Mueller polarimeter [75]. The best approach to study these samples is using a microscopy-like setup that allows a space resolved determination of the Mueller matrix [47, 69, 76]. The results of these measurements are images or maps of the optical properties, with a spatial resolution that can reach the micrometric range (diffraction limited). The high magnification is usually achieved using microscope objectives with strain-free characteristics and adapted to the wavelength of measurement.

There are two basic approaches to obtain space-resolved Mueller matrix images of a medium. One uses a multi-detector (CCD) that directly captures the image of the sample and the other uses a single point detector but the sample (mounted in an automatic x-y translator) is mapped sequentially to create maps of the optical properties. Both methods have its own advantages and drawbacks, but for chirality assessment the mapping approach is more convenient since the fast modulation frequencies of PEMs ($\sim$ 50 kHz) is incompatible with the relative low speeds of CCD detectors available today. To sort this difficulty some complex strategies to integrate modulation cycles of the PEMs for use with CCDs have been published in recent years [77,78]. However, these are methods of very difficult application, and most of them suited for instruments using one single PEM.

Single point detectors such as photomultiplier tubes (PMTs) are the most suitable to work with PEMs. . In a mapping measurement each Mueller matrix becomes one “pixel” of the resulting image. In order to have a high lateral resolution with this method only light that has passed through a tiny portion of the sample must reach the detector. This can be done either by reducing the size of the light spot impinging the sample or by placing a pinhole in front of the PMT. Scanning point by point a sample can be a time consuming process but PEM-based Mueller matrix measurements are quite fast (one measurement with 3 averages is collected in about 100 ms) so in less than 20 minutes it is usually possible to collect maps with 10000 points, which are usually enough to get an idea of the spatial features of a sample. Fig. 3 shows the chiral domains of opposite handedness formed in polycrystalline film of benzyl when it is grown from the melt.

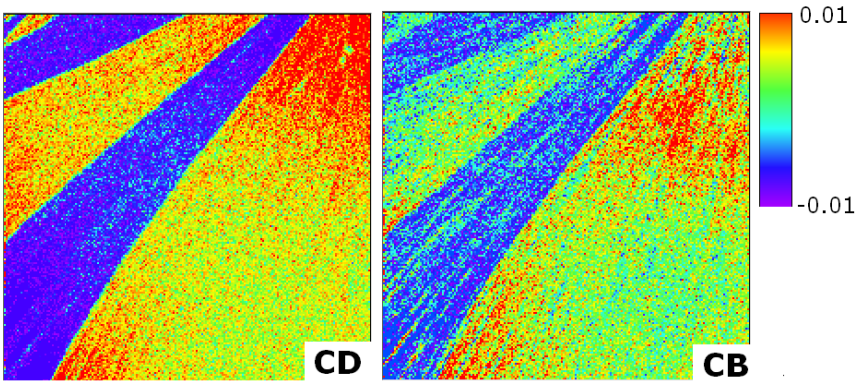

Fig. 3.3. Values at 400 nm of CD, CB, for benzyl grown from polycrystalline melt. Scans are 100 x 100 microns (by O. Arteaga from ref. 76).

The mapping technique also permits to cover systems with a large area that maybe do not require high resolution, but offer a very complicate response that cannot be understood from a single measurement. One example of this is the induction and switching of chirality in solutions of certain nanophases under the effect of a stirring vortex [79]. In these experiments the handedness of the induced optical activity depends on direction of stirring in a completely reversible process. Experiments were performed in ~ 10 mm pathlength cuvettes that were stirred using small magnetic bars. Cuvettes containing J-aggregates of different types of porphyrins have been investigated, showing an intense induction and switch of optical activity (usually easily traceable using CD and CB signals). Space resolved measurements in square section cuvettes, have revealed that the induction of optical activity takes place in the central part of the cuvette (see Fig. 4), in coincidence with the central chiral descending vortex.

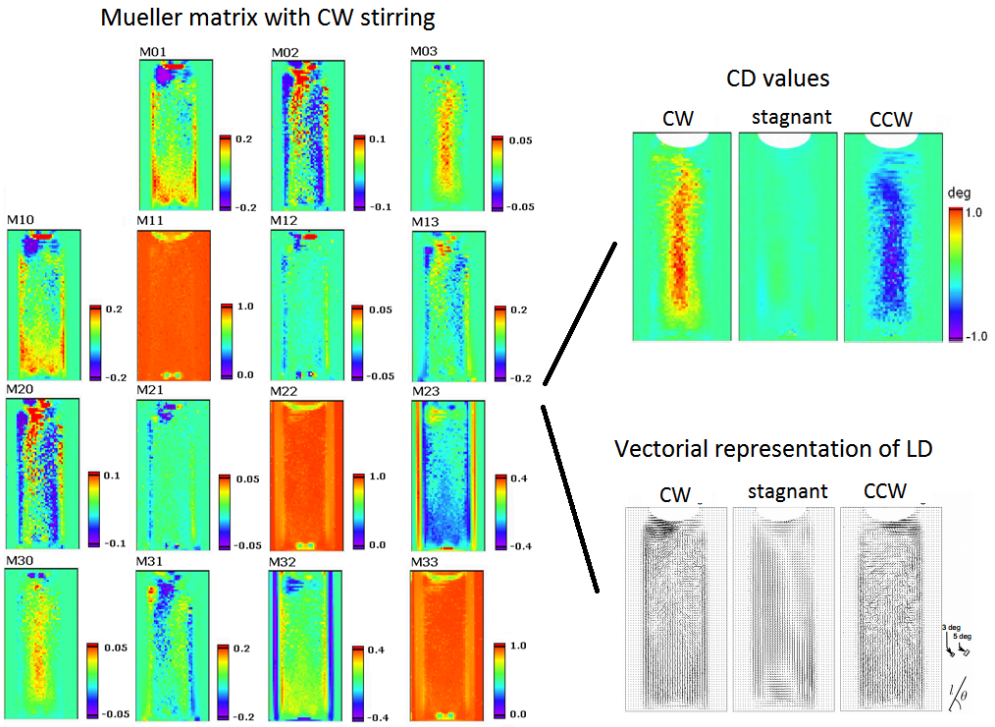

Fig. 3.4. (Left) Normalized spatially resolved Mueller matrix of clockwise (CW) stirred solution of J-aggregates measured at 485 nm. The dimension of each frame is 29 mm x 14.4 mm. (Right) CD and LD values as obtained from the Mueller matrix for CW, CCW stirring and in stagnant conditions. Adapted from Ref. 79.

4.- Conceptual optical design

4.1 Source properties

The photons are generated from a bending magnet which provides a source size of 133.3 μm and 76.4 μm FWHM horizontally (H) and vertically(V), respectively. As the critical energy of Alba is 8.5 keV, the flux at low energies is smaller that at a few keV. Panel a of figure 4.1 shows the spectral brilliance (ph/s mrad^2 0.1%BW) from 0 to 100 eV at 100 mA storage ring current.

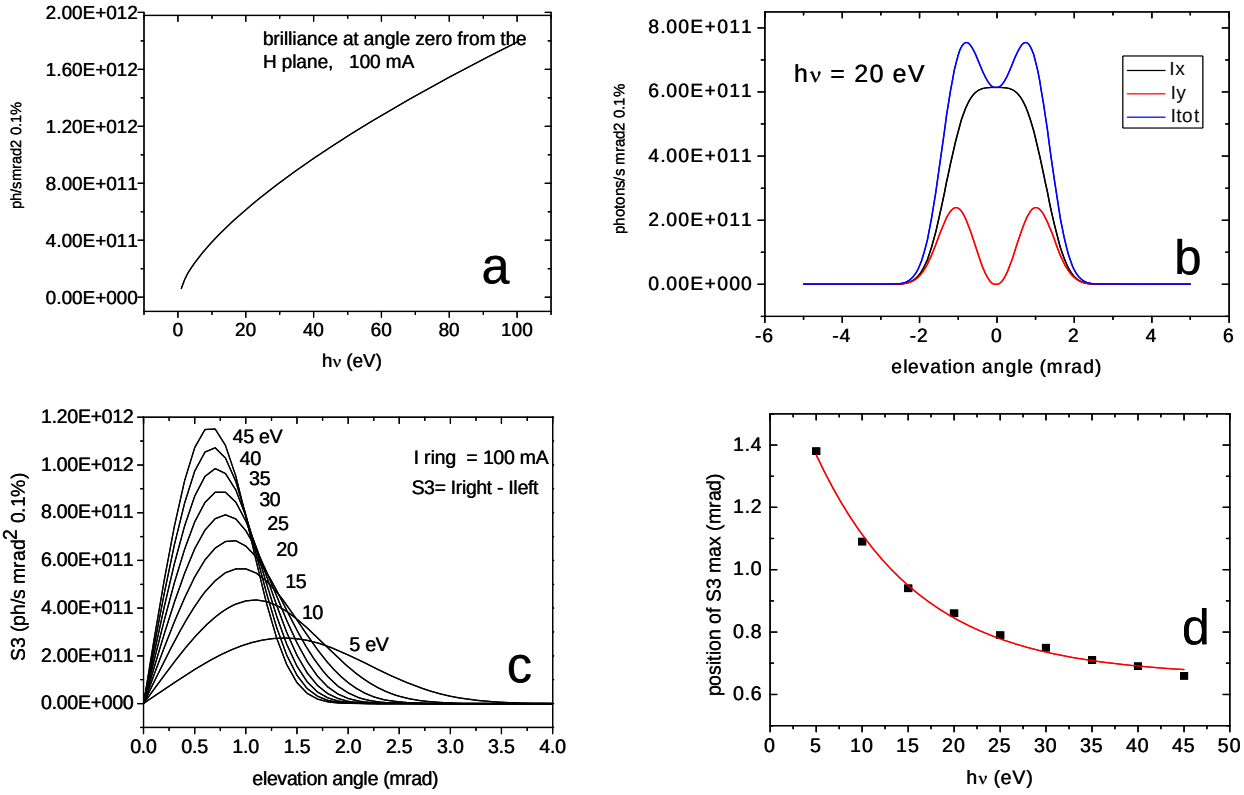

Figure 4.1. Some characteristics of the bending magnet source

Panel b displays an angular beam profile at hν = 20 eV along the vertical direction normal to the plane of the ring. Ix and Iy refer to the spectral brilliance for horizontal and vertical polarized radiation. For that particular energy, the intensity of vertical polarized radiation is zero in the orbit plane and shows two maxima at approximately ±1mrad .
The curves have been calculated with the software form the Center for X ray Optics at ALS.
Following Walker [80] the Stokes parameters are written as:

$$S0 = Ix+Iy \qquad S1 = Ix-Iy \qquad S2=0 \qquad S3 = \pm 2\sqrt{IxIy}$$

These are non normalized parameters and therefore S0 is the total spectral flux,
S1 is for horizontally polarized light and S3 for circularly polarized radiation
right (+) or left handed (-).
Panel c in figure 4.1 shows the intensity profile of the circularly polarized radiation for positive angles where I_{right} largely dominates. At negative angles a symmetric curve is obtained for I_{left} . The intensity profile of the circular polarization becomes sharper at higher energies and the position of the maximum shifts towards low angles as illustrated in panel d. Figure 4.2 further illustrates the distribution of circular polarization in a extended energy range.

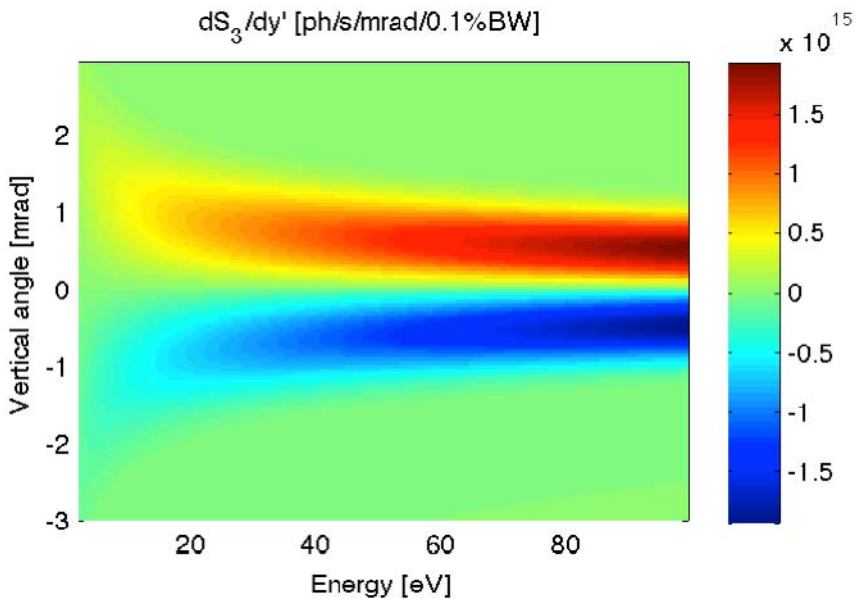

Figure 4.2. S3 component of the vertical angular distribution of spectral flux for the ALBA bending magnet, in the photon energy range of Skiron

The spectral flux (S_0), as well as its circular polarization component (S_3), integrated for all emission angles above the plane of the orbit is shown in Figure 4.3. A horizontal acceptance of 3 mrad has been considered.

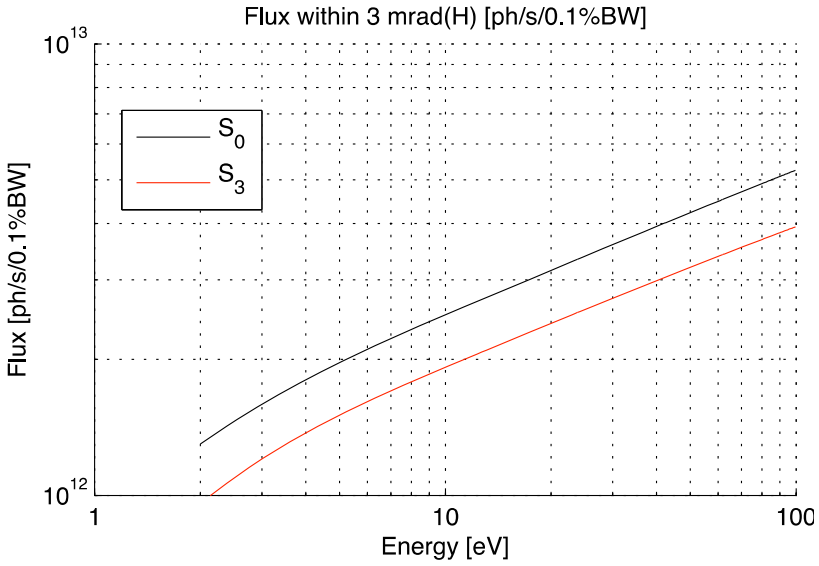

Figure 1.3. Spectral flux density emitted by the ALBA bending magnet, in the energy range of Skiron.

4.2 Basic optical concept.

The basic idea in the optical design of Skiron is inspired in that of Mistral at Alba and it is depicted in figure 4.4.

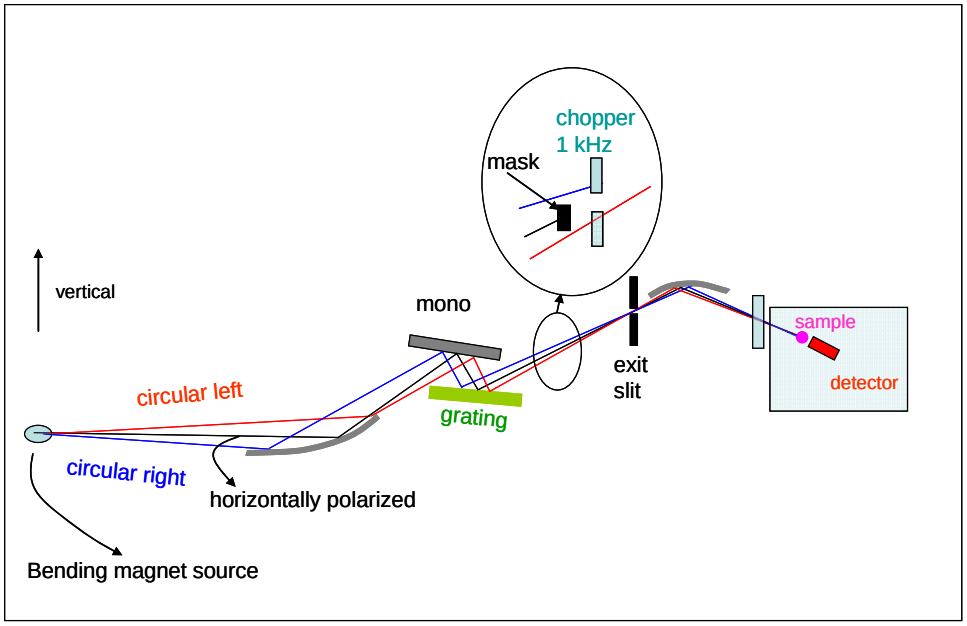

Figure 4.4. Basic conceptual optical design of Skiron

The bending magnet radiation is collected by a mirror with large acceptance to reflect the linear polarization (black ray) and both circular polarizations (red and blue). In the previous design of Mistral [81] this concept was also considered in order to have the possibility to perform magnetic circular dichroism measurements . In that case the mirror had to be 1200 mm in length due to the glazing incidence angle.
In fact, the name Skiron to design this beamline was chosen because is the Greek name of the northwest wind that in Spanish is Mistral.
Referring to figure 4.4, the radiation is monochromatized with a grating and after the monochromator a movable mask blocks the central part of the beam i.e. the planar polarization part. Then, a fast chopper transmits either the right or left handed circular polarizations which are focused to the sample. The chopper should ideally be fast (1 kHz is a good value). The importance of chopping fast will be discussed in 5.3. The signal at the detector after the sample, will be modulated at the chopper frequency and the amplitude of its Fourier component will be extracted either by using a Lock-In amplifier or by numerical analysis .
Note that the beam propagates under vacuum from the source to the sample and that there is nothing that intercepts it except the sample. The focusing and monochromatization are achieved with reflecting optics i.e. there are no filters or windows that the beam has to transverse. Due to this, the photon energy range is wider than the CD beamlines mentioned in table 1 which operate using photoelastic modulators, filters and windows.

In addition, the optical design has to allow using planar polarization by retrieving the mask.

After several considerations, it was decided not to use a vertically dispersing optics as that sketched in Fig. 4.4 but an horizontally dispersive one as described in what follows.

4.3 Optical design

4.3.1 General considerations

The main design goal of the optics of the Skiron beamline is to accept both polarization modes emitted by the ALBA bending magnet, and to preserve the polarization of the source until the sample in the most stable possible way.
The main difficulty for this lies in the fact that for grazing incidence, meridionally focusing optics, rays that impinge at different longitudinal positions of the mirror, have a different incidence angles. This variation has two effects, a small, usually negligible change in reflectivity, and a spatial variation of the photon density of the outgoing beam along the meridional plane, simply due to the different geometric projections of the beam.
In the case of vertically deflecting mirrors, photons emitted above and below the orbit plane, i.e. circular left and right polarizations, would impinge on the upstream and downstream sides of the mirror, and would be reflected (if the mirror is curved) with different photon density, on the defocused beam, for the two circular polarization modes.
In principle such asymmetry is not noticeable at the positions where the beam is focused, i.e. the sample or the exit slit. However, since the beam is defocused at its intersection with the optical elements, the two polarization modes would see different aberrations, and would still introduce differences for the two polarization modes at the sample positions.
Alternatively, sagittal focusing does not present this inconvenience, but it is not possible to have an aberration free optics with sagittal focusing only. This limits the spot size at the exit slit, (and therefore the resolution and photon throughput of the monochromator), and on the sample.
Taking this in consideration, we propose a beamline design with the following characteristics:

- It maximizes the symmetry of the beamline with respect to the (horizontal) orbit-plane, this is, having the minimum possible number of vertically focusing elements. In particular, the dispersion plane is horizontal.
- By this, all the mirrors with a role in the monochromator are meridionally focusing plano-elliptic mirrors. This allows minimizing the aberrations of the spot at the exit slit plane.
- The beamline includes also a pair of vertically deflecting mirrors. One of them is flat, and the other one has very long focal distance. Although this introduces a slight asymmetry between the two polarization modes, it is very small, and more convenient that using a sagittal focusing of the vertical plane. In addition since all

the other optical elements are horizontally deflecting, such asymmetry is not amplified by further aberrations.

- The beam is focused both vertically and horizontally at the exit slit. In that position the beam is cut only in the horizontal direction. But the vertical focus is also required to avoid having the two polarization modes spatially separated, being susceptible of an uneven transmission due to some geometric misalignment.
- In addition, the beamline includes provisions to compensate for manufacturing tolerances that would imply astigmatism or other aberrations on the exit slit focus. For that reason vertical and horizontal focusing is completely decoupled, using different mirrors, which are plane in their sagittal directions.
- In the same vein, the proposed plano-elliptic mirrors are motorized bendable ones. This allows doing a fine adjustment of the focus position without displacing the beam footprint on the mirror.
- Also in this sense, a plane mirror has been included in the monochromator, to be able to fine adjust the included angle on the grating.

In addition to these characteristics, which are directly derived from the polarization symmetry requirements, the beamline must provide the following functionalities

- It must have a large vertical acceptance, to accept the fully circular polarization emission for the whole energy range.
- It must also have a large horizontal acceptance, to maximize the flux on sample.
- It must be able to scan the whole energy range between 4 eV and 60 eV with the same grating, in reasonable time and without introducing any geometric change of the optics.
- It must maximize the photon density on the sample jet, which is vertical and about 10 μm thick.
- It must fit within the space of a bending magnet beamline at the Alba experimental hall. This has a tight requirement on the minimum distance from the source and the maximum transversal displacement from it.

These characteristics condition the optical design of the beamline, which is presented in more detail in the following sections.

4.3.2 Layout

The layout of optical design of Skiron is schematically given in Figure 4.5. The radiation from the bending magnet is vertically deviated by M1, which is flat. M1 absorbs most of the power of the source. The beam is deflected back onto the horizontal plane by M2. It is is a plano-elliptic bendable mirror that focuses the source vertically onto the exit slit plane. Downstream, M3 focuses the beam horizontally onto the entrance slit. M3 is also a plane-elliptic mirror. Downstream the exit slit, a flat mirror, M4, deviates the beam towards the grating, which is spherical. The grating focuses the beam horizontally onto the exit slit plane, where the beam is already converging. Downstream the exit slit, the beam finds first the chopper, and then a KB mirror pair (M6, M7) that focus the beam onto the sample. Alternatively, a retractable flat mirror is inserted onto the beam path upstream M5. It deviates the beam towards the low energy branch, for which additional focusing is done with MgF_2 transmission optics.

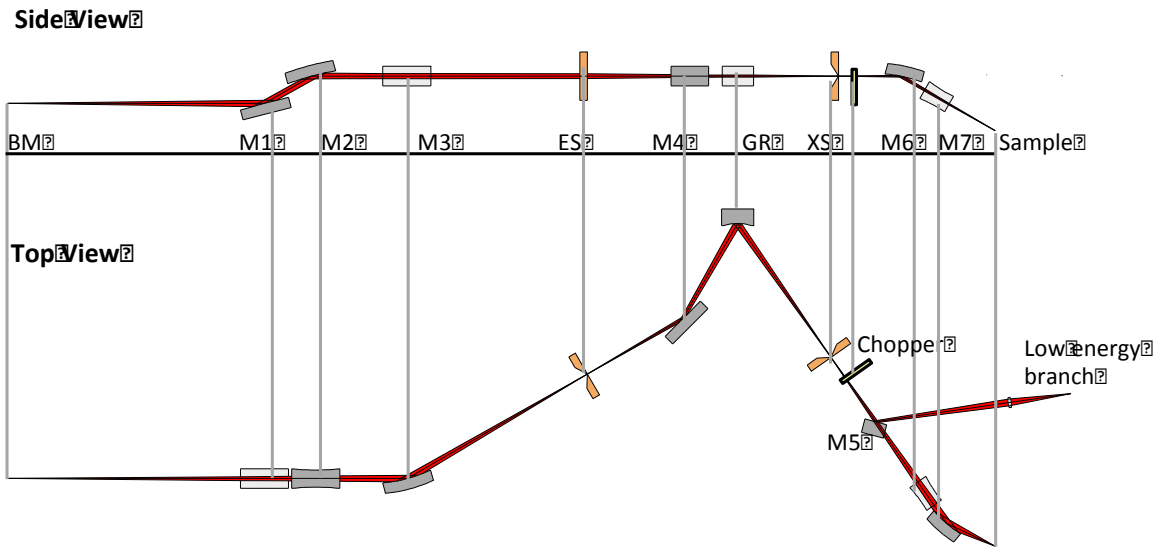

Figure 4.5 . Schematic layout of the the Skiron beamline

The proposed layout for Skiron includes large horizontal deflections, mainly by the grating. Thus, the beamline develops almost perpendicularly to the usual (and foreseen) beamline direction. Nevertheless, the resulting layout fits within the ALBA experimental hall without affecting any of the neighbor beamlines. Figure 4.6, shows how the proposed layout would fit as BL07 at ALBA. The positions of M3 and the entrance slit are actually determined by the need to have a long distance from the tunnel wall.
Other considerations we have taken into account in the design of the optical layout of Skiron are angular acceptance, polarization, aberrations, etc. These are discussed in the following sections.

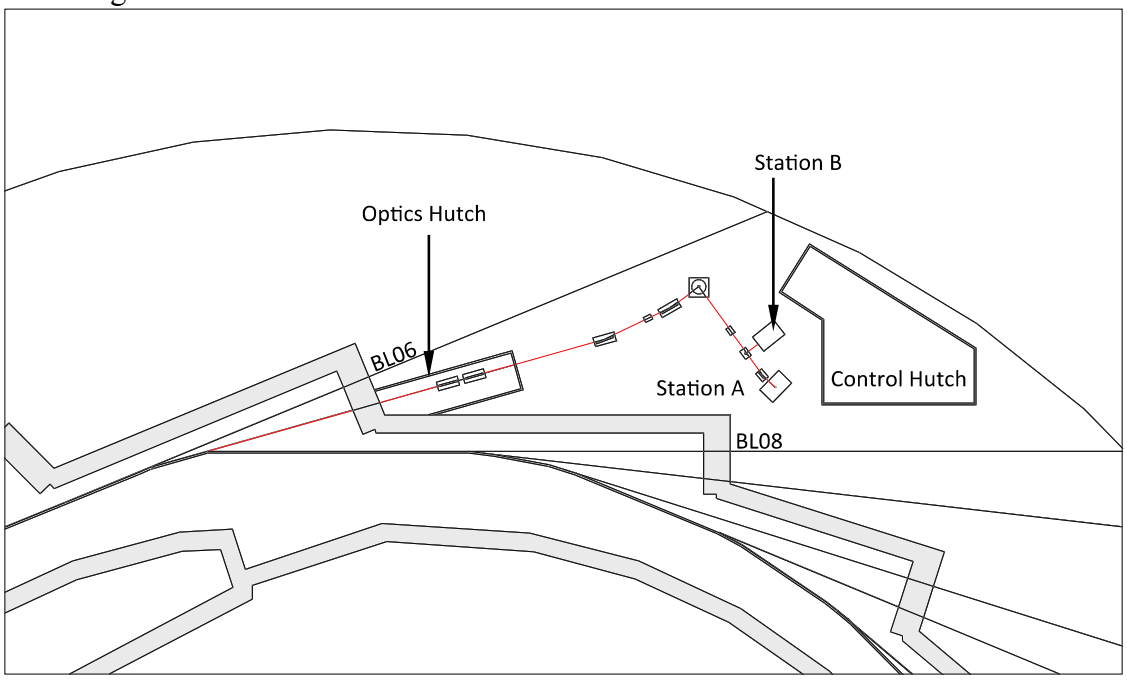

Figure 4.6 . Layout of the Skiron beamline at the BL07 position in the ALBA experimental hall.

4.3.3 Mirror Reflectivity

The reflective coating materials and incidence angles of the mirrors for Skiron have been selected to cut-off photons with energy above 60 eV, as well as to preserve as much as possible the polarization of the photons of the source.
The material chosen for the reflective coating is Aluminum, at an incidence angle of 5 deg. The corresponding reflectivity is shown in Figure 4.7. Although for that material and angle the cutoff energy is well above 60 eV, the reflectivity is actually limited by the absorption edge at 72 eV. The selected incidence angle is a good compromise to have similar reflectivity for the *s* and *p* polarization modes, which differ mainly at the low energy end of the beamline. Note that reflectivity near unity can be reached in a significant range of energies.

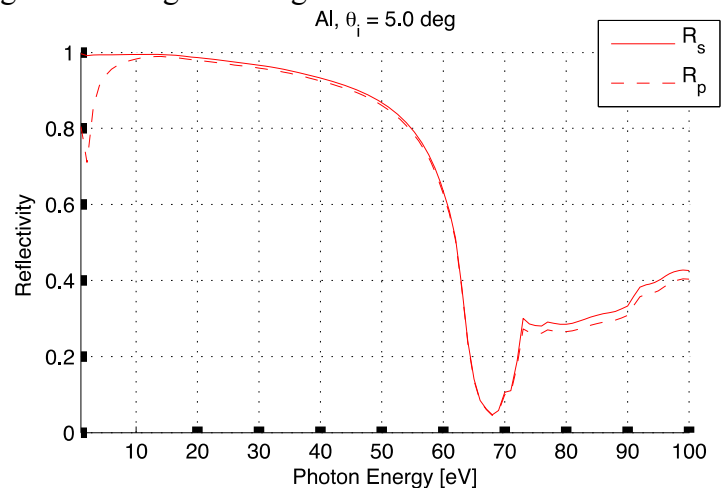

Figure 4.7. Reflectivity of Al in the photon energy range of Skiron, at an incidence angle of 5 deg.

Besides the different reflectivity of the two polarization components, one needs to consider also the relative wave retardation introduced by each reflection, which are significant for the energy range of Skiron. At each reflection, the phase difference between the two polarization components of the emitted field, which is originally one quarter of a wave, is modified, and may even vanish for some photon energies. In such case the resulting photons would be linearly polarized, what represents an effective reduction of reflectivity for the circular polarization components. This is illustrated in Figure 4.8 . It shows the spectral flux emitted by the Alba bending magnet, after four reflections on Al-coated mirrors, with incidence angles of 5 deg, all of them in horizontal deflection. The curves integrate all angles above the plane of the orbit. The black and red lines represent the S_0 and S_3 components of the Stokes vector, for the reflected radiation, respectively. One can see that even if the flux (S_0) is well transmitted for all energies, the S_3 component vanishes at about 7 eV, indicating that no circular polarization is transmitted.

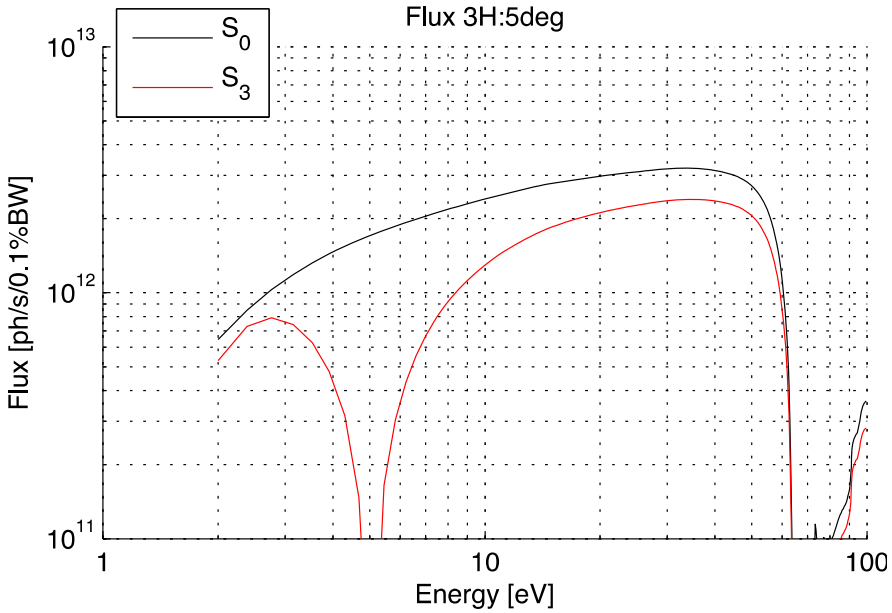

Figure 4.8. Spectral flux after three reflections in horizontal deflection mode, using Al-coated mirrors at 5 deg incidence angles.

To avoid this situation, we have introduced two vertical reflections, with incidence angle of 8 deg, to compensate the delay between polarization components, and to avoid loosing the circular polarization at some parts of the energy range of the beamline. The resulting flux spectrum is represented in Figure 4.9 One can see that most of the circular polarization is preserved after the five reflections.

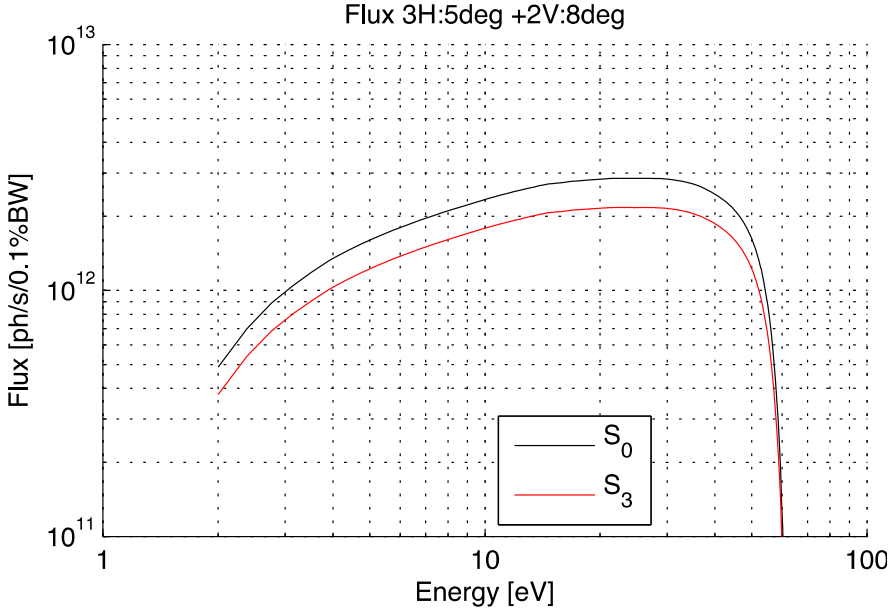

Figure 4.9 . Spectral flux after three horizontal reflections at 5 deg, and two vertical reflections at 10 deg,

4.3.4 Monochromator

Horizontal dispersion

Since the grating has to be scanned during experiments, it is not possible to completely remove the aberrations it introduces for the whole energy range of the beamline. By using a horizontal deflection scheme, we make sure that both polarization modes impinge symmetrically at both sides of the meridional axis of the grating. By doing this, the aberrations it introduces are also symmetric with respect to the horizontal plane and allow for equal transmission of both polarization modes.

Spherical grating

In order to have a large acceptance, the source is focused horizontally on the entrance slit plane, and the grating is placed at a relatively short distance from it. This allows reducing the footprint on the grating, which is the optical element with a tighter size limitation.
Because of this the beam incident on the grating is divergent, and needs to be re-focused on the exit slit. The simplest option is to use a curved grating surface. Any other option would require additional focusing elements between the entrance slit and exit slit. In addition, the energy range of Skiron allows using close to normal incidence, which reduces the effect of aberrations induced by the spherical grating.

Normal incidence

A near-normal incidence monochromator is required to have acceptable diffraction efficiency of both polarization components at the energy range required for the beamline, as well as to minimize the aberrations introduced by the grating. A fixed included angle of 90 degrees has been found to have acceptable efficiency for circular polarization modes in the whole energy range of the monochromator. Although smaller included angles have fewer aberrations and better efficiency for low energies, they cannot reach the high energy end of the beamline. More grazing incidences have better efficiencies for the *s*-polarization, but much lower for the *p*-polarization. In addition aberrations are more severe in these conditions. The diffraction efficiency for the chosen configuration is shown in Figure 4.10 The red line shows the diffraction efficiency for circularly polarized light. One can see that the same grating can cover the whole photon energy range of the beamline.

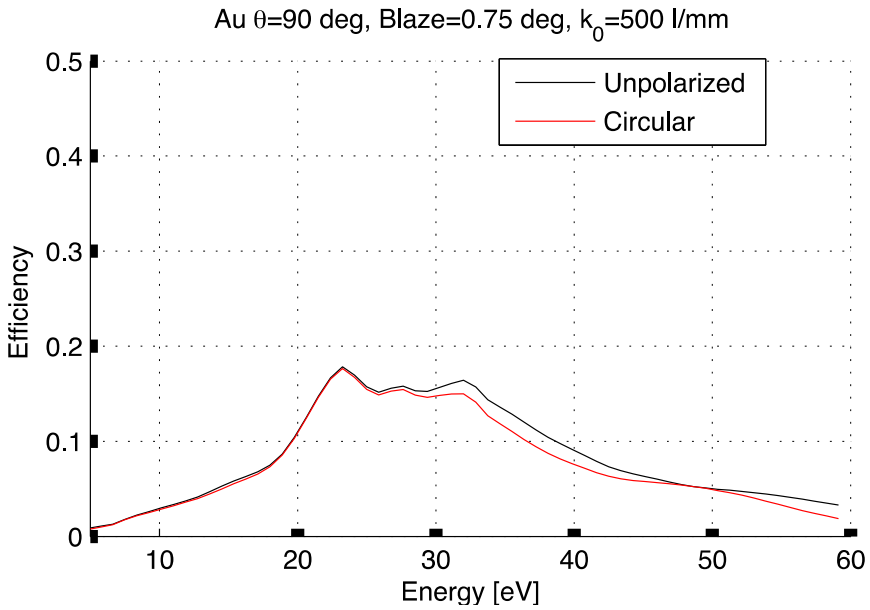

Figure 4.10. Diffraction efficiency for a gold coated, 500 l/mm blaze grating in a fixed included angle geometry of 90 deg.

Fixed included angle

Fixed included angle geometry has been chosen for the monochromator, for the simplicity of scanning energy by one single rotation. Due to the normal incidence, there is no need to compensate defocusing introduced by the grating. This saves from scanning a second motor, for instance to scan some slit position, as for the DRAGON type monochromators, or using a VLS grating, subject to tight manufacturing requirements.
The rotation required to cover the energy range of the beamline is 11.82 deg, which can be achieved by a simple lever arm mechanism.
Although the operation is foreseen at fixed included angle, we have included a flat mirror (M4) upstream the grating to fine adjust the included angle on the grating and to accurately match it to the actual radius of curvature of the grating.

4.3.5 Slits

Diagnostics-only entrance slit

Although the beam is horizontally focused on the entrance slit, there is not any beam limiting aperture at that position during operation. This is because at that position the beam is not vertically focused, and a small roll-mismatch between the slit and the preceding optics would cause an asymmetric cut of the upper and the lower part of the beam, with different impact on the polarization modes.

Exit slit

The beam is focused at the exit slit both vertically and horizontally. Considering that the dispersion is horizontal, the vertical focus of the beam does not need to be placed exactly at the exit slit. Nevertheless, it is convenient to focus it there in order to minimize the effect of a potential roll misalignment of the slit, which could cause a difference in the transmission of the two circular polarization modes.

4.3.6 Modulation of the polarization

The modulation of the polarization during the experiments is done by alternatively blocking the upper or lower part of the light cone, by means of a chopper placed ~300 mm downstream the exit slit. At position, the points of the transversal plane are well mapped to the angular coordinates of the emission cone. Figure 4.11 shows the projection of a 3×6 mrad^2 grid, at the source plane, onto the chopper plane. One can see that the grid is almost free of any optical distortion. The only distortion along the vertical direction is a small quadratic variation of the mapping scale.

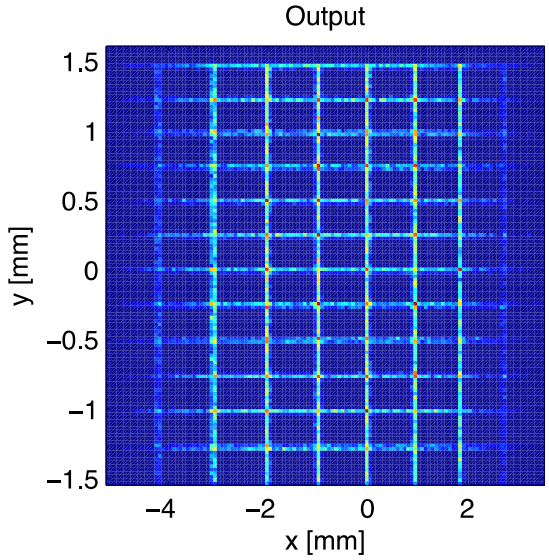

Figure 4.11. Mapping of the angular coordinates of the emission cone onto the coordinates of the chopper plane.

An example of how the polarization state is modulated by the chopper is given in Figure 4.12. We consider that the chopper is a slit that oscillates vertically following a sinusoidal function of time, with amplitude of 1.5 mm. The aperture of the chopper is also 2 mm. The flux, the degree of circular polarization (S_3/S_0) and the depolarization are given for one period of the chopper, as a function of time. We consider a photon energy of 4 eV. One can see that the polarization reaches almost the fully circular polarization modes even for that low energy. In addition the depolarization, which behaves as background for the dichroic signal is always below 20%. One can see also that the total flux presents an oscillation. This is due to the non-uniform emission profile of the bending magnet along the vertical direction for such low energies. One can also see that these oscillations are not completely equal for the first and second half of the cycle. This is due to the

remaining (but small) distortion of the mapping between the chopper plane and the directions of the emission cone.

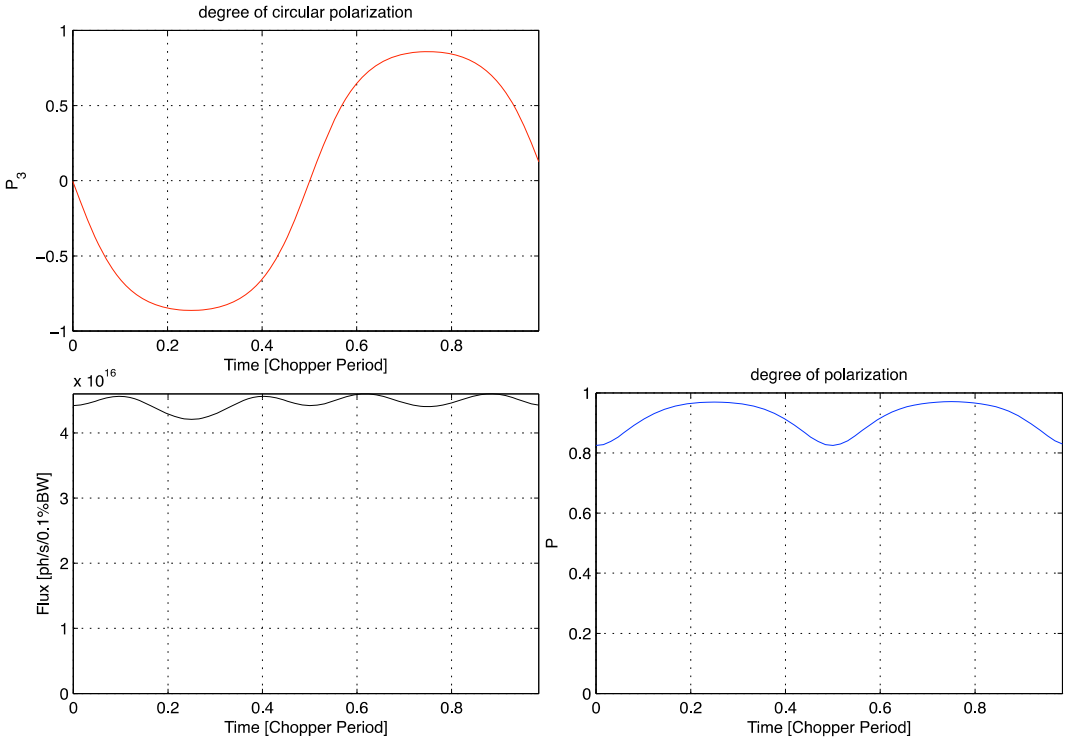

Figure 4.12. Modulation of the polarization at Skiron. Degree of circular polarization, flux and degree of polarization variation along one cycle of the chopper, calculated for 4 eV.

4.3.7 Refocusing optics

The refocusing optics is a KB mirror pair. The VFM optics is placed upstream and works in a smoother demagnification than the HFM. The resulting spot, assuming a slope error of 0.3μrad is given in Figure 4.13. The size of the focused beam is 17×32 μm^2 . Note that, resulting from the horizontal dispersion of the monochromator, the spot is much smaller in the horizontal direction than in the vertical. This suggests that the sample jet should travel in vertical direction. Another reason for this is to have a system more robust to potential defocusing of the beam on the simple.

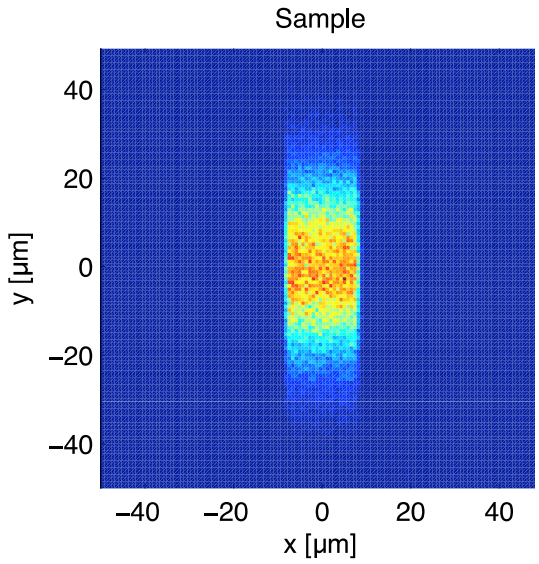

Figure 4.13 . Spot size on the sample plane, for a slope error of 0.3µrad on the mirrors

4.3.8 Performance

The resulting performances expected for the beamline are obtained by a ray tracing simulation. Figure 4.14 provides the resolving power for a gap of the exit slit of 20 µm. Note that resolution is much better at the low energy end of the beamline

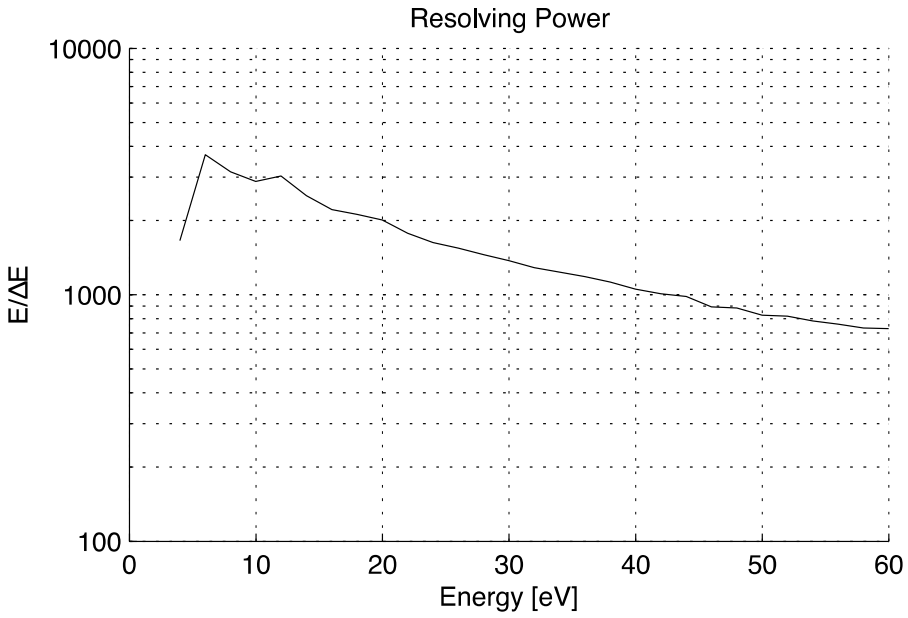

.

Figure 4.14 . Resolving power of the Skiron beamline for an opening of the exit slit of 20 µm.

The flux on simple resulting from the simulation is given in Figure 4.15. The curves represented in there provide the flux in photons per second, at the resolution achieved by the beamline, indicated in Figure 4.14. The black curve corresponds to the flux with a grating that can cover the whole energy range of the beamline without zeros in the S3

component, as mentioned above. The red curve corresponds to a grating with enhanced efficiency at the low energies, although it presents oscillations corresponding to inversions of the S3 parameters.

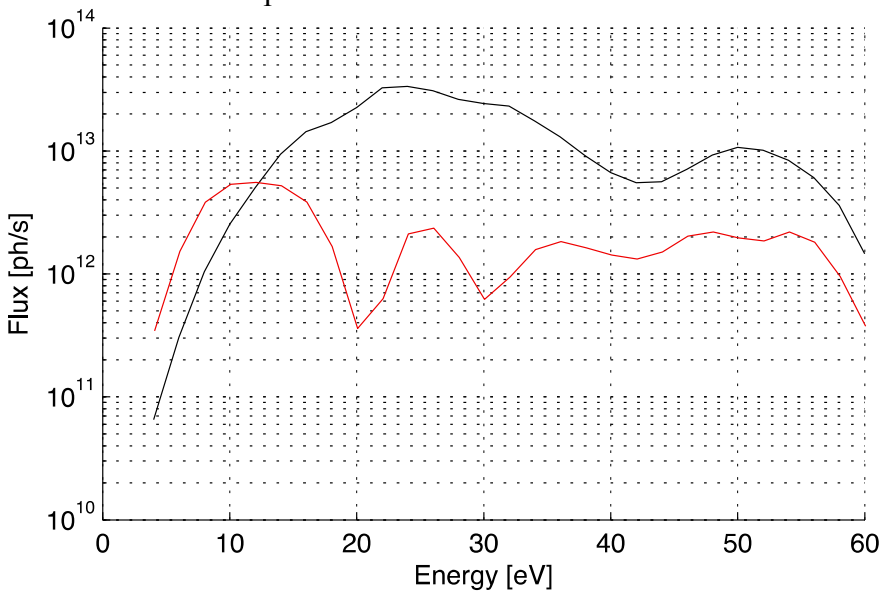

Figure 4.15. Flux on sample, at the actual resolution. The black curve corresponds to a grating without inversions of the S_3 component. The red curve corresponds to a grating with high efficiency for the low energies.

5.- Instrumental aspects

5.1 Statistics of measurements of weak CD signals

The natural CD signals from solutions of gas samples are in general small and the measurement of the dichroic signals faces the difficulty achieving enough statistical level to acquire significance. In order to have an idea of the necessary signal levels required for the measurement of specific CD signals we have assumed that they obey Poisson statistics:

$$D = \frac{I_R - I_L}{I_R + I_L} \qquad \sigma_R = \sqrt{I_R} \qquad \sigma_L = \sqrt{I_L}$$

$$\sigma_D = \sqrt{{\sigma_L}^2 \frac{4{I_R}^2}{(I_R + I_L)^2} + {\sigma_R}^2 \frac{4{I_L}^2}{(I_R + I_L)^2}}$$

The following graph plots D/σ_D vs the number of counts of one of the two channels:

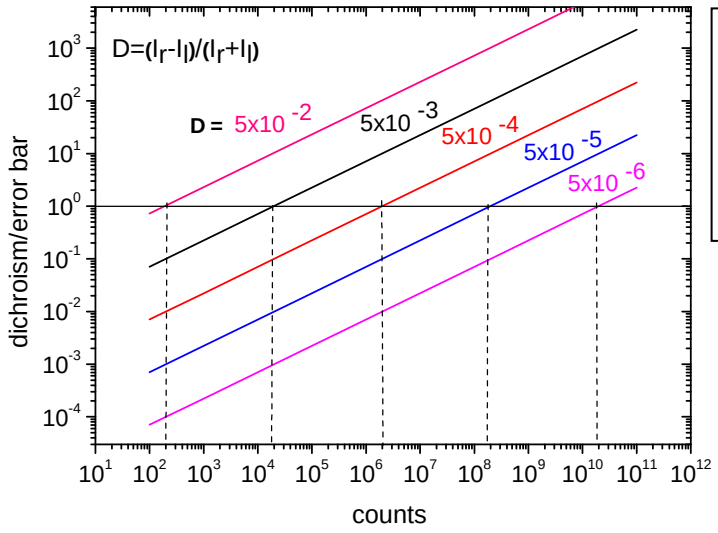

Figure 5.1.

Plot of the CD signal divided by its uncertainty as a function of the total intensity.

The horizontal line drawn at 1 is the threshold for observing a significant CD level. For example a dichroic signal of 0.05 requires 200 events to have a signal to noise (S/N) value of 1. To measure a dichroism of 0.005 , $2x10^4$ events are required. i.e. a ten fold decrease of the dichroic signal necessitates a 100 fold increase in the signal level as expected from Poisson statistics. The above figure accounts for statistical errors only. In practice other source of uncertainties or systematic errors dominate the accuracy of the measurements.

As example let us look the first experiment in asymmetric photoemission performed at Bessy with gas phase camphor molecules.[82]
The authors utilized photons from a bending magnet source and selected the circularly polarized radiation by inserting a slit above or below the orbital plane in the conventional manner. They quoted $1.2x10^{12}$ ph/s with a circular polarization rate of 0.92. The energy resolution of the experiment was 1%. They sublimated camphor and used an

effusive source to generate a Maxwellian gas beam. The photoelectrons were collected by an electrostatic analyzer with a total acceptance angle of 14° and there were amplified with a channeltron electron multiplier. They acquired signal until reaching a total of 10^6 counts/s in the spectra (1-5 minutes acquisition time) which resulted in measured dichroic photoemission signals around 0.04 with error bars about 0.005 which corresponds to S/N ≅ 8 . In figure xx D= 5 x10^{-2} and S/N = 8 corresponds to N= 2x10^4 counts significantly lower than the reported value. This seems to indicate that it is not the statistics linked to the photon flux who determines the accuracy of the experiment.

5.2. Electron detection.

As the photoelectron current from macromolecules in solution the liquid jet is expected to be very small, a high transmission electron energy analyzer is necessary even at expenses of energy resolution.

The best energy resolving electron analyzer in terms of transmission has been recently implemented at Bessy and applied to pump probe experiments in liquid jets. It is a time of flight detector (TOF) [85,86] coupled to a magnetic bottle [84] which allows to collect 2π stereorad solid angle. The instrument requires a photon pulsed source with pulse widths of less than 1 ns which are delivered either by pulsed laser sources or storage rings operated in single bunch or hybrid mode.

As an example, if the slowest electrons that one wishes to detect have a kinetic energy of 4 eV, their flight time through a path of 60 cm is 506 ns that has to be shorter than the repetition rate of the photon pulses in order to avoid the overlapping of electrons generated in consecutive pulses. As the circumference of Alba is ca. 300 m and the period of revolution of a single electron packet is 1000 ns, then, an hybrid mode of operation of filling ½ of the ring with "normal" electron bunches separated by ~2ns and the other half containing only a single electron packet would be satisfactory. The electron energy resolution is linked to the temporal extension of the electron bunch . For ΔE/E = 0.01 , 0.8 ns would be sufficient for resolving 40.0 eV and 40.4 eV electrons. This means in practice that even if the natural length of 20 ps of the electrons pulses at Alba is doubled or triplicated due to the "special" filling mode, the pulse length would not affect the energy resolution.

The largest advantage of TOF detectors is that their transmission is about 3 orders of magnitude higher that conventional electrostatic electron analyzers which are generally used in photoemission as for example the hemispherical analyzer Scienta R3000 [83], that has high energy resolution at expenses of transmission. The disadvantage of TOFs is the requirement of a pulsed (less than 1 ns) photon source which might not be available.

If for some reason TOF is not considered as the first option, an intermediate solution between TOF and hemispherical analyzers is the Cylindrical Mirror Analyzer which has about 100 times more transmission than the hemispherical at expenses of a relatively low resolution (E/ΔE = 200 instead of 1000-5000 of hemispherical).

5.3 Photon helicity switching

As mentioned above, the natural CD effect has magnitudes of the order of 10^{-4} or less which are difficult to measure. A relevant work that we wish to comment was carried out by Prumper et al. [87] at Bessy and Elettra using helical undulators that periodically switched the circular polarization from right to left handed. The authors measured total and partial ionization yields of two aminoacids (alanine and serine) in the gas phase both in the vacuum ultraviolet region (hν = 10 - 32 eV approximately) and at the C1s edge. The authors could not detect any circular dichroism larger than 10^{-3} due to the ±0.1 % error bars of their measurements. The overall result of the article was to set an upper limit of the CD effect. Its article reads:

"*…The (photon) helicity can be inverted every 5 s. This is a crucial feature in order to perform CD measurements with an accuracy of better than* 10^{-3}*, because this way, a slow change in the target density does not influence significantly the ratio of the count rates for* σ^+ *and* σ^- *light.*"

At present all the operating beamlines that switch the circular polarization of the photons operate at flipping frequencies of a few Hz, examples are:

DESIRS (Soleil) [24] : ca. 1 Hz ; Circular Polarization Elettra [88] ca. 0.05 Hz ; Bessy ca. 150 Hz (tests only) [89] ; Polux (SLS) [90] 1 Hz (10 Hz in future), …

At NSLS II there is a project of a beamline for fast polarization switching based on two canted Apple undulators [91] . It aims to switch the helicity at a maximum rate of 1kHz and it will be implemented in the phase II of the beamline project in the next few years.

The fundamental principle of the fast switching consist in acquiring a CD datum (difference from R and L helicities) faster than the rates of change of physical variables (photon flux, beam position, electron orbit feedback corrections, electronic noise, mechanical vibrations…) that might affect the result of the measurement . If the helicity switching frequency is high enough, the externally changing variables look static and do not influence the result, in other words, Fourier filtering allows to effectively isolate the signal at the switching frequency since it is well separated from the undesired low frequency components.

Some typical frequencies that enter into play are: a) the electron orbit feedback system of Alba operates at 150 Hz therefore one expects beam oscillations at this and higher frequencies. The horizontal beam instabilities are much more pronounced that the vertical ones. This is a fortunate circumstance in a bending magnet beamline that is almost insensible to horizontal beam displacements . b) The electronic noise appears typically at 50 Hz and at higher harmonics, c) the vibrations of the mechanical parts as linear motions, supports etc.. are in practice below 100 Hz, d) the vibrations induced by mechanical fore pumps are in the range 50-100 Hz whereas that of, say, a 1200 l/s turbomolecular pumps is about 630 Hz.

Another argument favoring high frequency chopping arises from the nature of the electronic noise. At low frequency the so called *1/f noise* that affects all electronic components dominates. However, at higher frequencies the *1/f* contribution becomes negligible, and the noise tends to become smaller and constant (*white noise*). The typical dependence of the noise amplitude with frequency in signal detection is shown in figure 5.2. The change of the slope of 1/f in the plot defines the so called corner frequency . Its value depends on the combination of several factors. Two of them are critical: the bandwidth of the acquisition electronics which increases the 1/f noise and the source resistance of the measure which increases the white noise level.. The value of 1 kHz in the figure corresponds to a fast amplifier as required and is far from the low order harmonics of the 50 Hz frequency of the mains.

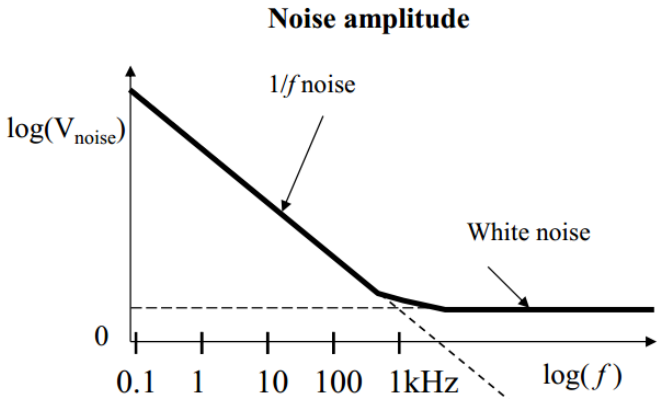

Figure 5.2 . Frequency dependence of the noise amplitude

If for example a lock-in has a bandwidth of 10 Hz (good lock-ins can be much better than this) it is easy to realize that the amount of noise affecting a measurement at 1 kHz will be much lower than if the measurement was done at only 10 Hz. The colored areas of Fig. 5.3 are a visual representation of the amount of noise collected by the lock-in during the measurement. In general it is advisable to work with modulation frequencies of at least 1 kHz. As once this threshold has been reached the noise distribution becomes quite constant, there is no much benefit in increasing the chopping speeds above a few kHz.

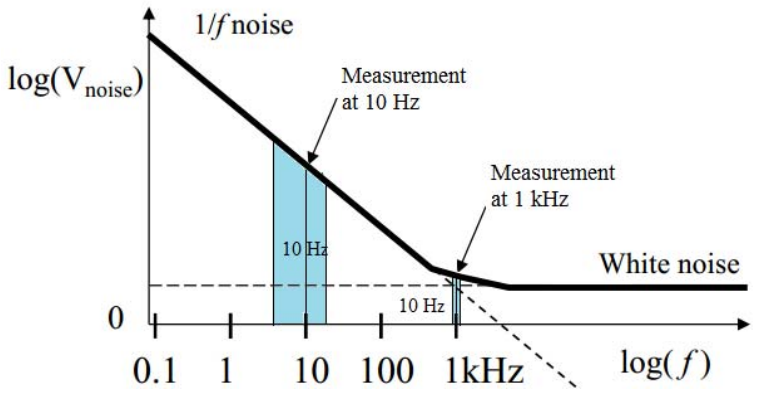

Figure 5.3
Noise discrimination with a 10 Hz band-pass filter at different modulation frequencies. Measurement at 1 kHz is much less affected by noise than the one at 10 Hz.

Consequently it would be desirable to switch the beam helicity at ~1 kHz .
As it will be described in more detail later, it is planned to equip Skiron with a high frequency chopper that will select R or L polarizations and that would allow to reach 10^{-4} or lower sensitivity levels in liquid and gas phase photoemission CD measurements.

5.4 End Station. Branch A

As discussed above, the end station will be based on a TOF+magnetic bottle detector and a capillary set up for producing liquid or gas jets.
The figure below outlines the main components of the end station of branch A

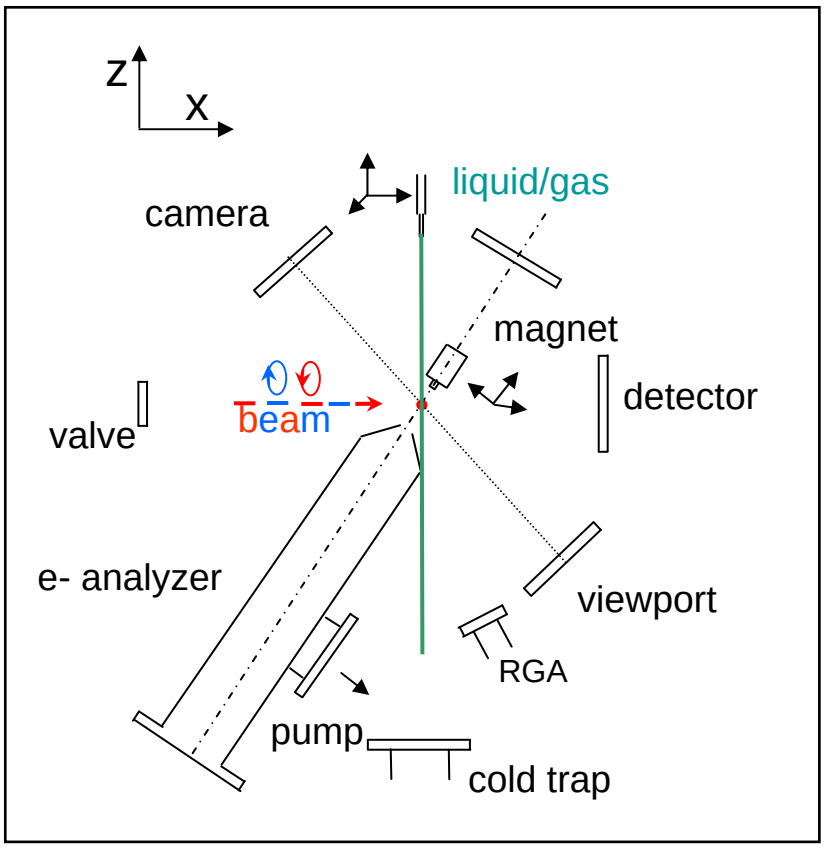

Figure 5.4: schematics of the end station of branch A showing the main components. The red dot signals the interaction region of the photon beam and the gas or liquid jet. The z axis is vertical.

A brief description of the main of the components follows.

- The photon beam after the exit slit transverses a differentially pumped stage (not shown) to maintain the UHV of the beamline optics.

- A valve separates the end station and the rest of the beamline

- A chopper will select right or left handed circularly polarized beams. The position of the chopper in the beamline is to be determined since it will depend on the detailed design of the optics. In the present optical design it is located after the exit slit. There are several possibilities for beam shoppers. We prefer in principle to operate with a piezoelectric resonator that has attached a small metal frame for obstructing the undesired polarization component. Usher et al. [92] report on the dynamics of piezoelectric actuators based on lead zirconate titanate. The authors report displacements of a small metal plate up to 1mm at resonance frequencies about 70 Hz. The operating frequency is far too low for our purposes and it is unclear how much can be increased with an appropriate design. This is a subject for in-house development work.
  Another interesting possibility is to use tuning fork shoppers commercially available that may operate at 1kHz with displacements of 1 mm. they are based on a mechanical resonator driven by a current coil. The shopper has to be installed in a x-y-z high precision stage to achieve well balanced circular beams.
  Traditional wheel type choppers are at present not considered due to their high mass which generates vibrations at or near the chopping frequency and to their demanding operating requirements.

- A detector in the direction of the photon beam will be used for beam control and Io monitor (phosphorous screen plus photodiode).

- An electron analyzer with an electron multiplier probably either a TOF or an electrostatic of cylindrical symmetry equipped with a skimmer at the entrance and differential pumping.

- A permanent magnet of few centimeters will be used to drive the photoelectrons to the entrance of the spectrometer. It has to generate a field of about 0.5 T and it has to be precisely positioned (three linear translations) and retractable. The implementation of this magnet it unclear at present and will require numerical simulations to verify its suitability.

- An optical system as a camera or a telescope will allow to properly adjust the geometry and to visualize the liquid jet

-The liquid jet system that also allows to be used for generating gas jets, will be purchased directly to the company MicroLiquids GmbH .

-A cold trap will condensate the liquid. It should be designed to allow recycling of already used liquid for expensive molecules in solutions.

- A residual gas analyzer will be used to control the gas composition in the

background.

During commissioning, the entrance valve will be substituted by a MgF2 window and at the position of the detector in the figure 5.4, the instrument of branch B will be installed to measure the Stokes parameters of the beam and to determine precisely its polarization. This operation will be carried out at atmospheric pressure (so the electron analyzer will be valved off or removed) and it will be limited to the wavelength range transmitted by the window.

5.5 End Station .Branch B

The 4-PEM branch of the beamline will be based on more conventional optical set up than the vacuum branch. Its configuration will be fully transmissive and it will use photoelastic modulators (PEMs) as key optical components. Its novelty will come from the fact that for the first time, to our knowledge, complete Mueller matrix spectroscopy will be realized with synchrotron radiation. The Mueller matrix polarimeter using 4-different PEMs was constructed for first time during 2012 using a small laboratory Xenon light source (220 nm-800 nm) [69]. The optical design of this bench-top laboratory system is summarized in Fig. 5. This is the faster and more precise full Mueller polarimeter constructed to date because it measures simultaneously all the 16 elements of the Mueller matrix without any moving part. In comparison, the instruments used worldwide to acquire CD spectra are limited to one single PEM and measure only one element of the Mueller matrix (M_{03}).

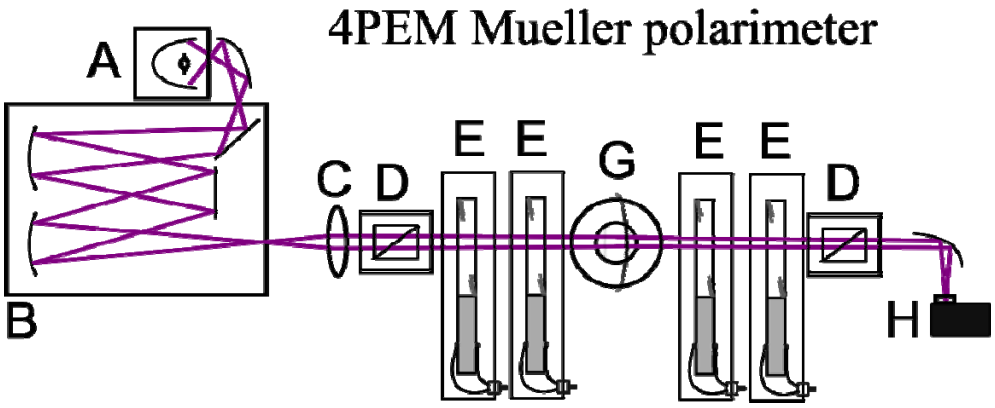

Fig. 5.5. Schematic drawing of the optical elements involved in the spectroscopic laboratory 4-PEM polarimeter. The light beam goes from left to right. A, Xenon arc lamp; B, Monochromator; C, collimating optics; D, polarizer; E, photoelastic modulator (PEM); G, sample holder with angular adjustments; H, photomultipler tube.

For visible and near-UV CD measurements, standard laboratory light sources such as Xenon arc lamps may be used. Below about 250nm, however, complications arise. First,

calcite polarizers such as Glan-Taylor types cannot be used. Magnesium fluoride polarizers such as Rochon types must be used which provide only a few degrees of separation between the two orthogonally linear polarized light beams. This complicates the setup that may be used for CD measurement by restricting the acceptance angle for light into the polarizer. Second, the brightness of Xenon lamps decreases rapidly with decreasing wavelength below 250nm. Some commercial CD instruments using arc lamp light sources are able to make measurements down to about 180 nm, but the photon flux at that point is much dismissed and any measurement becomes highly affected by noise. Deuterium lamps might be used in this region but these are extended sources with relatively low intrinsic brightness. Synchrotron radiation is ideal for CD measurements or, more generally, Mueller matrix measurements because it has very high intrinsic brightness, is highly directional, is linearly polarized and has a continuous spectral intensity distribution.

The synchrotron 4-PEM Mueller polarimeter we propose is going to make use of the linearly polarized radiation part of the beamline. The optical heads of the PEMs will made of CaF_2 (transparent down to 130 nm), with two PEMs placed before the sample and the other two after the sample. To access to all elements of the Mueller matrix all four PEMs need have different frequencies of resonance [69]. The angular misalignment between contiguous PEMs is going to be 45^o. After the last PEM another polarizer is used before the light goes to the detector assembly. For the analyzer we propose to use a MgF_2 Rochon Prism as this material offers transmission in the deep UV (down to 125 nm).

5.5.1 Photoelastic modulators

As already outlined in xxx, photoelastic modulators (PEMs) are polarization modulation devices that utilize the photoelastic effect to provide modulation of the polarization state of a light beam. The device may be thought of as a waveplate with fixed retardation axis and sinusoidal varying retardation amplitude. Unlike many other types of polarization modulators, PEMs can be built o cover a wide spectral range: from the vacuum UV (about 120 nm) to the mid-IR (about 16 microns) [93]. They are used in a wide variety of applications such as Stokes polarimetry, ellipsometry, measurement of birefringence, measurement of optical rotation and reflectance difference spectroscopy, etc.

A PEM is composed of an optically transparent material with a high elasto-optic efficiency and low mechanical dissipation (e.g. fused quartz, CaF_2) and of an oscillating

piezoelectric transducer. The light beam passes through the optical element which is mechanically stressed by a periodic strain variation (typically at 20-80 kHz) by the transducer. This oscillating stress causes changes in the refractive index of the optical element, which exhibits a birefringence proportional to the strain. Fig 5. Show a photo of a quartz PEM, in which the optical element and the transducer can be clearly distinguished.

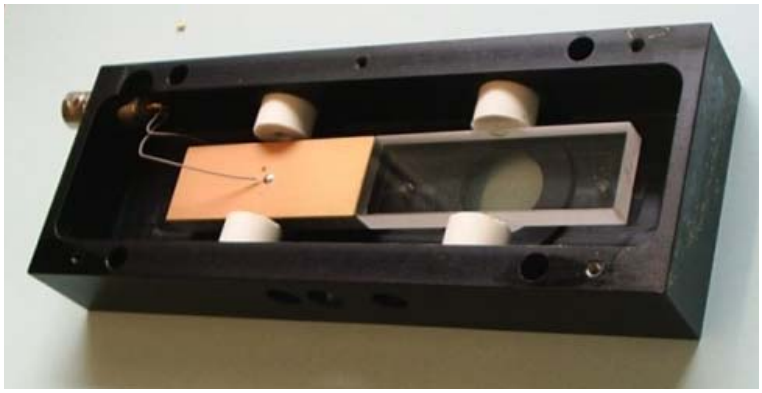

Fig. 5.6. Photo of a PEM with its case opened. The strain in the transparent optical element depends on the voltage given to the transducer.

As a result of its design, a PEM has unique optical features, such as high modulation purity and efficiency, broad spectral range, high power handling capability, large acceptance angle, large useful aperture and high retardation stability [93]. These features make the PEM the best choice for synchrotron polarization modulation in applications that require high sensitivity, because it offers a modulation quality unsurpassed by other types of electro-optic modulators or liquid crystal modulators.

5.5.2 Spectral Range

Any transmissive optical element present in this branch of Skiron (photoelastic modulators, polarizers, windows, etc) needs to be transparent in the deep UV. The most common materials employed in CD synchrotron beamlines are LiF, Mg_2F and Ca_2F. These materials are insulators with electronic band gaps of 13.6 eV (91 nm) , 10.8 eV (115 nm) and ~12.0 eV (103 nm) respectively. The percent transmissions for 5 mm thick samples in the UV are:

Material	λ = 120 nm	λ = 220 nm
LiF	50	90
Mg_2F	60	92
Ca_2F	5	92

Table 5.2. Transmittance (in %) of different materials at 120 nm and 220 nm

As mentioned above these values of the transmission is what effectively limits the lowest wavelength achievable in practice.

Another important experimental aspect is the absorption by the air and water vapor which is very significant in the far UV as illustrated in Fig. 2. The transmission of air has a deep minimum at around 21 eV (59 nm) which arises from the intense absorption bands of N2 and O2 at 21.7 eV (57.1 nm) and 20.8 eV (59.6 nm) respectively. For water vapor another deep minimum occurs at 19.9 eV (62.3 nm). As a consequence measurements in the far UV region below ca. 130 nm require minimization of air path. The convenience of minimizing the air path has been already been considered and implemented by Gekko et al. [94] which designed an experimental set up where the sample is inside a vacuum chamber that is directly connected to the vacuum of the photoelastic modulator chamber

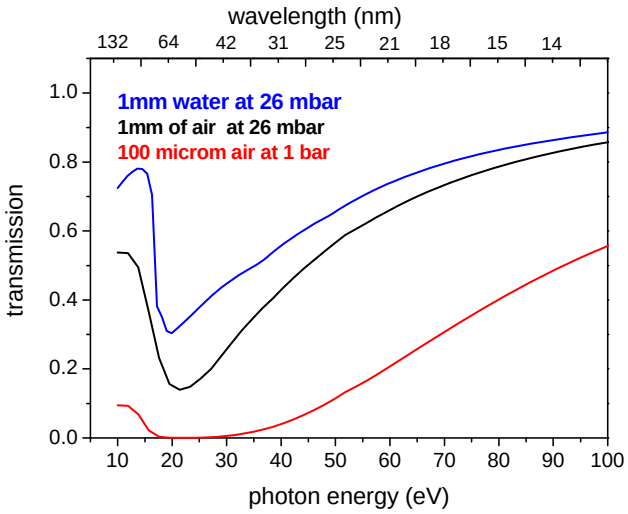

Fig. 5.7. Transmission of 1mm of air and water vapor at 26 mbar and of 0.1 mm of air at 1 bar vs photon energy and wavelength. (The wavelengths in the top axis have been rounded to 0 decimal places).

Given these constraints we anticipate that the lower wavelength limit for the 4-PEM transmissive branch of Skiron will be around 130-135 nm.

5.5.3 Data analysis

The signal detected by the photomultiplier shows a rather complex time-dependency because it contains multiple Fourier harmonics with frequencies that are linear combinations of the frequencies of modulation of the PEMs. With a phase-sensitive Fourier analysis of the intensity waveform, 16 independent parameters that correspond to 16 elements of the Mueller matrix are simultaneously extracted. The values of the Mueller matrix element can be obtained from the amplitude of certain harmonics, while the sign can be retrieved from the phase .

A 16-bit digitizer is fed with the amplified signal of the PMT signal and the four reference signals coming from the PEMs. All five signals are acquired synchronously using a random software trigger. Since each PEM has at its own frequency (ω_i) and phase (ϕ_i), the first step of the data acquisition procedure is a FFT to determine these two parameters from the square reference signal coming from one of the PEMs. The common frequencies available for PEMs manufactured by Hinds Instruments are approximately (±200Hz) is ω_0=50 kHz, ω_1=60 kHz, ω_2=42 kHz, and ω_3=47 kHz, while the phases change at each data acquisition. The data processing system uses a synchronous filtering algorithm that works like 16 digital lock-in working in parallel, one for every Mueller matrix element. All the details about the theory behind the acquisition and data processing system are available in Ref. [69]. We anticipate that the calibration procedures described there will be directly applicable for the synchrotron 4-PEM polarimeter. Probably the only major difference will come from the fact that the synchrotron polarimeter will be operated under vacuum conditions and it will require to use of some optical windows in the path. The effect of such windows on the polarization of light, even if minimal, will need to be calibrated in order to be removed from the measure.

5.5.4 Targeted Specifications

In table 5.3 we summarize the specification we anticipate for the 4-PEM polarimetric branch of Skiron

Characteristic	**Expected Value**
Resolution	0.0005 ^{o} (CD), 0.001 ^{o} (other optical properties)
Reproducibility	0.0008 ^{o} (CD), 0.002 ^{o} (other optical properties)
Accuracy	0.001^{o} (CD), 0.002 ^{o} (other optical properties)
Wavelength range	130nm-400 nm
PEMs optical head material	CaF_2
CD max value	±20^{o}
Measured quantities	CD, CB, LB, LD and depolarization
Throughput (time estimation for a Mueller matrix measurement)	0.1s

Table 5.3. Targeted specifications of the synchrotron Mueller polarimeter.

6.- Estimated cost (kilo euro)

	kilo euro
Front end	165
Personnel Safety System	76
Optics hutch	100
Fluids	50
Mechanical installations	80
Electrical installations	52
Conventional hutch (including furniture and climatization)	38
Computing equipment and infrastrucure (cables, network, PLC, icepaps, computers..)	78
Computing and control: External Manpower	68
Mechanical hardware (frames, motion…)	150
Vacuum components (pumps , valves , gauges)	175
Diagnostics	50
Optics: monochromator	250
Optics : M1,M2, M3, M4 and M5 mirrors and mechanics	750
Optics: M6-M7 mirrors KB pair	180
End station A	
Electron analyzer with electronics	170
Vacuum chamber and positioning hardware	60
Turbo pums and roughing (2)	40
Liquid jet complete set up	55
Diagnostics detector and mounting	25
Ancillary	50
End station B	
4 PEM	92
Optics harware (windows, filters optomechanics ..)	17
Detector	18
Optical table	40

Precision mechanics	11
Computers and control	11
Ancillary	25
Total	2876
Contingency 10%	288
TOTAL	**3163**

7.- Potential Users and scientific impact.

In terms of users of Skiron, both branches are clearly different.

Branch B should compete with advantage with the laboratory equipments since it would provide enhanced photon flux as it has been already mentioned before. If only one PEM device were used, branch B would very similar to other existing beamlines devoted to CD spectroscopy and therefore it would be of general usage to users that utilize CD spectroscopy as a standard characterization tool. In Spain there are at present 30 commercial equipments from Jasco in operation [95] . Their distribution is the following:

U Autonoma Madrid - Ctro. Biología Molecular Severo Ochoa
Universidad de Sevilla – F. Ciencias – Química Inorgánica
U La Laguna - Instituto Universitario de Bio-Orgánica (IUBO)
U La Laguna - F. Biología - Biología Animal
U Autonoma Barcelona - F. de Ciencias - Servei d'Anàlisi Química
U Santiago Compostela - F. Química - Química Orgánica
U Granada - F. Ciencias - Química Física
U Complutense Madrid - F. Químicas - Bioquímica
U Alcala Henares - F. Ciencias - Química Física
U Granada - F. Ciencias - Química Física
U Alcala Henares - F. Farmacia - Química Física
Universitat de Barcelona - Serveis Suport Recerca
U Santiago Compostela - F. Química - Química Orgánica
U Miguel Hernandez - Inst. Biología Molecular y Celular
U Almeria - F. Ciencias Experimentales - Área Bioquímica y Biología Molecular
Universitat de Barcelona - Serveis Suport Recerca
Inst. de Química Orgánica General – CSIC
CIC BioGUNE-Biología Estructural
Universidad de Oviedo. – F. Química –Química Física
Centro de Investigaciones Biológicas – CSIC

Universidad de A Coruña - Servicios Centrales de Investigación
Universidade de Vigo - Centro de Apoyo Científico y Tecnológico a la Investigación (CACTI)
U Malaga - Servicios Centrales de Apoyo a la Investigación (SCAI)
Universidad de Sevilla CSIC - Inst. Bioquímica Vegetal y Fotosíntesis
CIC NanoGUNE Consolider
UDL - Universitat de Lleida
CIC biomaGUNE
U Autonoma Madrid - F. Ciencias - Química Orgánica
U Granada - Ctro. Instrumentación Científica
Universidad de Córdoba - El Servicio Central de Apoyo a la Investigación (SCAI)

They are installed in Universities or laboratories of the CSIC and many of them are used as services for biology or organic chemistry departments.
In principle all the users of these equipments might be users of Branch B.
If a time resolved stop flow experimental set up is added, then, less standard spectroscopic measurements could be performed attracting more users.
Branch B in its standard operating mode with 4 PEMs for polarimetry, would attract additional users as those involved in anisotropic systems as fibrils with an ordering direction or adsorbed layers on ultrathin metal layers. Probably new opportunities and ideas will emerge from complete Mueller matrix determination.

Branch A involves unprecedented experiments in liquid photoemission from solutions at relatively high UV photon energies. The experimental results are expected to open new avenues and produce significant advances in the understanding of optical activity of transitions involving deep molecular orbitals.
Similarly gas phase experiments, although less original than the liquid jet ones, would allow to investigate how chirality in the molecular level is "transported" or modified by the molecular interactions of different chemical species.

Overall we believe that branch A will stimulate and attract scientists at international level.

8. Letters of support

Instituto Universitario de Investigación
Biocomputación y Física
de Sistemas Complejos
Universidad Zaragoza

Zaragoza, 09/01/2014

Prof. Javier Sancho
Department of Biochemistry, Molecular and Cell Biology
Biocomputation and Complex System Physics Institute
University of Zaragoza.

Scientific opportunities of the proposed Skiron beamline at Alba

The research in our group deals with structural and kinetic studies of proteins in solution (e.g. protein stability, folding and binding), with applications in Medicine. CD spectroscopy is commonly used to characterize the conformational properties of biomolecules and I believe its potential exceeds its present use in the field.

The Skiron project devoted to CD in unprecedented conditions opens very interesting scenarios.

Branch A:

The possibility to perform CD spectroscopy at wavelengths below 180 nm might be of importance in determining new structural data on the secondary structure of proteins which are poorly known at present. The usual deconvolution of far-UV spectra in helix, strands and coil could be greatly improved and extended to finer classifications if a larger spectral window were used. This could help to establish the fold of the proteins analyzed.
A challenging practical aspect concerns the amount of sample required to acquire good spectra. Liquid jet photoemission is a promising tool for studying radiation sensitive molecules in solution in the far UV. As the technique is very recent, the first experiments should be performed with commercial proteins which are non expensive and abundant. However, as the most important samples have high economic cost , it is essential that the experimental set up be designed in a way that samples could be re-circulated. This is considered a "must".

Branch B:

An important application that branch B opens up is the study of protein fibers (essential for the understanding of the characteristic aggregates observed in amyloide diseases such as Alzheimer disease) which are forced to have defined orientations. The linear dichroism (LD) spectra would provide additional information to the CD spectra as for example the side chain orientation of specific amino acids and the arrangement of the strands within the fibrils.
The simultaneous CD and LD spectra that Skiron will allow will be a powerful advanced spectroscopic tool that, as far as we know, it is not available at present.

In summary, in my opinion Skiron would offer new and important opportunities in the field of CD which makes this beamline very attractive for our group.

Sincerely

Javier Sancho

Salvador Ventura
Chair Professor of Biochemistry and Molecular Biology
ICREA Academia
Head of the Protein Folding and Conformational Diseases Lab (PFCD)
Institute of Biotechnology and Biomedicine
Dept. of Biochemistry and Molecular Biology
Parc de Recerca UAB, Mòdul B
Universitat Autònoma de Barcelona
E-08193 Bellaterra (Barcelona)
E-mail: salvador.ventura@uab.es

Sept 2014

Expression of interest of our Group in the proposed Skiron beamline.

Introduction.

Our research group is intensively investigating the impact of conformational changes in proteins on the regulation of their functional properties and the relationship between these changes and human disease. The CD spectroscopy technique is one of our standard tools to investigate the structural and binding properties of both natural and disease-linked protein variants. Despite certain conventional laboratory CD instruments allow to perform kinetics in the ms time scale, their lack of light intensity make that they require relatively high protein concentrations, which usually results in side aggregation reactions preventing measurement in low wavelengths and the attainment of reliable kinetic constants, specially when the reactions are very fast. The Skiron beamline would overcome these difficulties opening exciting possibilities.

Stopped flow technique

In this technique, solutions are forced from syringes into a mixing chamber. After a very short period of flow, the flow is stopped suddenly and measuring is triggered. A stopped flow instrument is in fact a rapid mixing device, and is used to study in solution the chemical kinetics of fast reactions that have half-lives as short as a few milliseconds. When instrument is coupled to either a circular dichroism spectrometer or a fluorescence spectrometer it becomes extremely useful in the field of protein folding and structure, to observe rapid unfolding and/or refolding reactions and the associated conformational changes in proteins.

Protein Folding

Protein folding is the ultimate process where the information contained in genes is transformed into the final functional unit, an active folded protein from the unfolded primary amino acid sequence. The spontaneous folding of proteins from their initially disordered states to attain the native structure or the partial or total unfolding of the functional conformation under stress conditions are usually very fast reactions that cannot be tracked by conventional approaches. In fact, whereas equilibrium analysis provides information on protein stability, only kinetic analysis using stopped-flow techniques can provide us information on the energetic barriers for folding and unfolding, which are the most relevant parameters to understand *in vivo* protein homeostasis. CD analysis is an ideal technique to obtain these data since the spectra of folded and unfolded proteins and peptides are usually very different.

Salvador Ventura
Chair Professor of Biochemistry and Molecular Biology
ICREA Academia
Head of the Protein Folding and Conformational Diseases Lab (PFCD)
Institute of Biotechnology and Biomedicine
Dept. of Biochemistry and Molecular Biology
Parc de Recerca UAB, Mòdul B
Universitat Autònoma de Barcelona
E-08193 Bellaterra (Barcelona)
E-mail: salvador.ventura@uab.es

Sept 2014

Expression of interest of our Group in the proposed Skiron beamline.

Introduction.

Our research group is intensively investigating the impact of conformational changes in proteins on the regulation of their functional properties and the relationship between these changes and human disease. The CD spectroscopy technique is one of our standard tools to investigate the structural and binding properties of both natural and disease-linked protein variants. Despite certain conventional laboratory CD instruments allow to perform kinetics in the ms time scale, their lack of light intensity make that they require relatively high protein concentrations, which usually results in side aggregation reactions preventing measurement in low wavelengths and the attainment of reliable kinetic constants, specially when the reactions are very fast. The Skiron beamline would overcome these difficulties opening exciting possibilities.

Stopped flow technique

In this technique, solutions are forced from syringes into a mixing chamber. After a very short period of flow, the flow is stopped suddenly and measuring is triggered. A stopped flow instrument is in fact a rapid mixing device, and is used to study in solution the chemical kinetics of fast reactions that have half-lives as short as a few milliseconds. When instrument is coupled to either a circular dichroism spectrometer or a fluorescence spectrometer it becomes extremely useful in the field of protein folding and structure, to observe rapid unfolding and/or refolding reactions and the associated conformational changes in proteins.

Protein Folding

Protein folding is the ultimate process where the information contained in genes is transformed into the final functional unit, an active folded protein from the unfolded primary amino acid sequence. The spontaneous folding of proteins from their initially disordered states to attain the native structure or the partial or total unfolding of the functional conformation under stress conditions are usually very fast reactions that cannot be tracked by conventional approaches. In fact, whereas equilibrium analysis provides information on protein stability, only kinetic analysis using stopped-flow techniques can provide us information on the energetic barriers for folding and unfolding, which are the most relevant parameters to understand *in vivo* protein homeostasis. CD analysis is an ideal technique to obtain these data since the spectra of folded and unfolded proteins and peptides are usually very different.

Universitat Autònoma de Barcelona

Knowing the early determinants of protein folding is highly relevant from the biomedical point of view since many human diseases are caused by mutations in proteins and biological peptides, which affect their rates of folding. CD is an excellent method to determine the structural changes caused by mutations and to determine how the mutations affect the rates of folding. Many folding diseases, including Creutzfeldt-Jakob disease (CJD), cystic fibrosis, and many cancers, involve relatively slow conformational changes that can easily be followed using CD. Understanding the difference in the folding process can bring insight into the causes of these diseases at the molecular level.
The early stages of folding determine in fact the fate of the protein in the cell, since during this time it is formed the so-called folding nucleus, which will drive all the subsequent folding reaction. The formation of this nucleus is usually accompanied by the induction of native-like secondary structure, a reaction that can be tracked by CD when this device is in line with stopped-flow instrument (Science. 1978 Jan 27;199(4327):425-6. Far-ultraviolet stopped-flow circular dichroism. Luchins J, Beychok S.). This technique also allows to track the transient formation of off-pathway folding intermediates that can lead to the accumulation of misfolded species able to self assembly into cytotoxic macromolecular structures known as amyloid fibrils and responsible of diseases like Alzheimer's and Parkinson, again a process that can be tracked using CD to monitor the formation of beta-sheet rich ensembles.

Other applications
In addition to the analysis of folding reactions the technique can provide unique information on the fast conformational protein changes occurring during protein binding to drugs and during protein-protein interactions an area of increasing interest since many proteins are being shown now to remain intrinsically disordered in the cell and only fold upon fast binding to their specific targets.

Conclusions
Our group is extremely interested in the Skiron beamline project, specially in what concerns time resolved CD in the ms range using stopped flow experiments since it would allow exploring areas of our research field that would remain obscure in the absence of this facility, despite they are perhaps the most relevant to understand the molecular determinants of protein folding and binding.

Best regards,

Salvador Ventura

Institut de Biotecnologia i de Biomedicina - Universitat Autònoma de Barcelona - 08193 Bellaterra (Cerdanyola del Vallès), Barcelona, Spain Tf. +34 93 581 1233 – Fax. +34 93 581 2011 ibb@uab.es http://ibb.uab.es

Letter of support for the SKIRON beamline proposal at the ALBA Synchrotron

By
David B. Amabilino
EPSRC/GSK Professor of Sustainable Chemistry
School of Chemistry
University of Nottingham
University Park
NG7 2RD
e-mail David.Amabilino@nottingham.ac.uk

11th September 2014

To whom it may concern

To be able to measure the optical activity – related with the chirality or handedness - of molecules on a surface would solve key questions such as how the interface influences the conformations of chiral molecules, how chiral molecules interact with each other and with guest species at a surface, or how molecular machines function at an interface. At present, there is no technique that allows one to study these phenomena accurately or with absolute confidence. A synchrotron source that could probe chirality in monolayers would comprise a major breakthrough and yield important fundamental understanding in all of these areas and others. For example, the technique might be used to detect biomolecules at interfaces.

Regarding the specific areas of interest of this supporter of the proposal, a real challenge at the present is to observe the chirality of monolayers on gold, and the interactions that they have with other compounds. Self-assembled monolayers on gold are the most widely kind of used surface assembly, but precise detail concerning chiral arrangements at their surfaces are not available. They are important because many of the applications that they are used for – sensing, separation, or hierarchical growth – need this kind of detail in order to be understood. Taking our own work as an example, we proved that chiral monolayers on gold were able to template the growth of crystals of a complementary chiral molecule[1] and that micropatterned layers of a similar – but not identical – type seemed to show diastereoselectivity in crystal growth.[2] However, at present we can only hypothesise about the role of the chiral groups in this process. Having precise dichroic information in a wide energy range would allow precise determination of conformation in the different layers, and to be able to correlate the selectivity with monolayer structure. This is not possible through diffraction techniques because of the lack of long range order in the layers.

And how do chiral molecular motors work on surfaces[3]? The same argument holds true for the analysis of these systems: The lack of long range order means that circular dichroism is a crucial technique. In this field the understanding of chiral conformation interconversion is critical to the development of the area that is a burgeoning one.

Apart from monolayers of gold, there are a whole range of self-assembled monolayer systems formed on glass, silicon, ITO and so on that could all benefit tremendously from

---

[1] A Chiral Self-Assembled Monolayer Derived from a Resolving Agent and its Performance as a Crystallization Template for an Organic Compound from Organic Solvents, A. Bejarano-Villafuerte, M. van der Meijden, M. Lingenfelder, K. Wurst,R.M. Kellogg, D.B. Amabilino, Chem. Eur. J., 2012, 18, 15984–15993.

[2] Chiral micropatterns for the crystallization of enantiomeric organic compounds from organic solutions, M. Lingenfelder, A. Bejarano-Villafuerte, M. van der Meijden, R.M. Kellogg, D.B. Amabilino, Chem. Eur. J., 2014, 20, 10466-10474.

[3] Controlled rotary motion of light-driven molecular motors assembled on a gold film, G.T. Carroll, M.M. Pollard, R. van Deldena, Ben L. Feringa, Chem. Sci., 2010,1, 97-101.

precise information on the chiral conformations at interfaces. Especially, biological systems at interfaces are extremely important,[4] since many cell adhesion and growth places take place at interfaces.

Self-assembled monolayers on graphite do form ordered structures, although domains are too small to be studied by diffraction techniques, but even so their complexes with chiral guests is an important area,[5] and circular dichroic information on the changes in molecular conformation when these binding events take place would enlighten the area. For layers on graphite very little is known concerning the orientation of self-assembled monolayers except indirect evidence from molecular modelling. The ability to observe a monolayer chirality into the far UV would enlighten the origin of the conformational changes that take place in these layers when they are forced into alternative orientations when compared to their preferred ones.[6]

The reactivity of chiral molecules at interfaces is a growing field and one of great importance for heterogeneous catalysis. Spectroscopies already yield considerable information on the processes taking place at interfaces, but they are unable to detect the reasons for stereoselectivity and therefore the design of efficient catalytic systems remains difficult. While the identity of different oxidation states in monolayers can be detected by spectroscopies and even by scanning tunnelling microscopy,[7] the observation of chiral conformational effects during catalysis would pinpoint the chemical mechanisms of the processes. Circular dichroism at interfaces where catalysis takes place is therefore also of transcendental importance.

It is clear that the SKIRON beamline if commissioned would provide crucial information for these areas of research that have been given by way of example, but also many others such as Langmuir layers or the adsorption of naturally occurring chiral molecules on bioinorganic surfaces. The facility would be unique in the world and would provide information unavailable through any other technique.

---

[4] Biomolecules at Interfaces – Chiral, Naturally. A. González-Campo, D.B. Amabilino. Top. Curr. Chem., 2013, 333, 109-156 (ISBN: 978-3-642-37625-2)

[5] Pasteurian segregation on a surface imaged in situ at the molecular level, H. Xu, W.J. Saletra, P. Iavicoli, B. Van Averbeke, E. Ghijsens, K.S. Mali, A.P.H.J. Schenning, D. Beljonne, R. Lazzaroni, D.B. Amabilino, S. De Feyter, Angew Chem Int. Ed., 2012, 51, 11981–11985.

[6] 'Sergeants-and-Corporals' principle in chiral induction at an interface. I. Destoop, H. Xu, C. Oliveras-González, E. Ghijsens, D.B. Amabilino, S. De Feyter, Chem. Commun., 2013, 49, 7477-7479.

[7] Detection of Different Oxidation States of Individual Manganese Porphyrins During their Reaction with Oxygen at a Solid/Liquid Interface, D. den Boer, M. Li, T. Habets, P. Iavicoli, A.E. Rowan, R.J.M. Nolte, S. Speller, D.B. Amabilino, S. De Feyter, J.A.A.W. Elemans, Nature Chemistry, 2013, 5, 621–627.

Dr. Christine Joblin
Senior scientist at CNRS
Institut de Recherche en Astrophysique et Planétologie
Université de Toulouse et CNRS
9, Av. du Colonel Roche
31028 Toulouse Cedex 04- France
Tel.: +33 (0)561 558 601 / Fax.: +33 (0)561 556 701
Email: christine.joblin@irap.omp.eu

Dr Salvador Ferrer,
ALBA Light Source
Cerdanyola del Vallès 08290
Spain

Toulouse, October 3rd 2014,

Object: Support letter for the Skiron project at ALBA

Dear Dr Salvador Ferrer,

Following our discussions, I am glad to send you this document, which describes our research activities on cosmic polycyclic aromatic hydrocarbons and the interest we find in the Skiron projet at ALBA for these activities, which are now mainly conducted in the framework of the ERC Synergy Grant project called Nanocosmos (2014-2020) that involves the CSIC-ICMM in Madrid as well. This letter got also the support of my collaborators and their groups, who are represented by Paul Mayer (University of Ottawa, Canada), Patrick Moretto-Capelle (LCAR, University of Toulouse and CNRS, France) and Serge Martin (ILM, University of Lyon 1 and CNRS, France). As described in the following document we would be very interested by the Skiron VUV beamline and the magnetic bottle electron spectrometer if the latter can be combined with a mass-over-charge analysis, which is necessary to address our science on molecular fragmentation.

Please do not hesitate to contact us for further information.

Sincerely yours,

Christine Joblin

Institut de Recherche en Astrophysique et Planétologie
CNRS - Université Paul SABATIER
9 avenue du Colonel Roche - Boîte postale 44346 - 31028 Toulouse Cedex 4
Tél. : 05 61 55 66 66 - Fax : 05 61 55 86 92

Cosmic polycyclic aromatic hydrocarbons using Skiron at ALBA

Scientific background

The research activities in my group focus on the understanding of cosmic polycyclic aromatic hydrocarbons (PAHs), their properties, how they are formed and how they evolve. These activities involve laboratory experiments, astronomical observations and modeling. Because of the extreme conditions that prevail in astrophysical environments (in general very low gas densities and temperatures) sophisticated laboratory experiments such as jet experiments and ion traps are needed to perform these studies. Another aspect is that VUV photons play a key role in the photophysics and chemical evolution of PAHs in space. They can induce ionization and/or photodissociation, the latter determines the survival of PAHs in these environments and can be a source of small molecular species such as H_2 and small hydrocarbons. These VUV photons cover energies up to 13.6 eV in molecular clouds, and ~20 eV and more in diffuse ionized regions surrounding young, hot stars. Synchrotron radiation is key for these studies since it provides VUV sources with broad tunability and relatively high photon flux.

Experimental approach

In Toulouse (IRAP), we have developed the PIRENEA setup, which consists in a cold ion trap, in which species can be isolated from their environment (thermal background and collisions). Photodissociation experiments are performed in a multiple photon scheme using a Xe arc lamp or an OPO laser at typical rates of 10 s^{-1} and in competition with IR cooling [1,2,3]. We have developed collaborations with several experimental groups to study the properties of PAHs. At the University of Ottawa (P. Mayer's group), the thermochemistry of PAH ions (activation energies and entropies, product ion enthalpies of formation) is studied by combining mass analyzed ion kinetic energy spectrometry and collision-induced dissociation mass spectrometry techniques [4,5,6]. In Lyon (ILM, S. Martin's group), PAH ions are isolated in an electrostatic storage ring (the Miniring). Hot ions are injected from the source and their internal energy distribution is probed via their fragmentation upon laser excitation. This allows us to quantify their radiative cooling, which is dominated by fluorescence from thermally excited electrons and not IR emission at high temperatures [7].

Related to these studies our recent experience with VUV synchrotron radiation made use of the SOLEIL and Swiss Light Source (SLS) facilities, at which imaging photoelectron-photoion coincidence (PEPICO) spectrometers are available. At SLS, the experiments led by P. Mayer are devoted to study the stability of PAH and dihydro-PAH cations [4,5,6,8].
On the VUV beamline DESIRS at SOLEIL, the PEPICO spectrometer DELICIOUS, which can now perform simultaneous mass-selected ion and electron imaging, was used to study the electronic properties and stability of PAH clusters [9]. Our next goal is to use ion trap setups to study the dissociation of PAH ions (dynamics and branching ratios). In photoelectron measurements, the same photon, in the range ~15-25 eV, is used to ionize and dissociate PAHs. These experiments explore very specific conditions and complementary studies in ion traps are required for a wider investigation of interstellar conditions. A research group from

Institut de Recherche en Astrophysique et Planétologie
CNRS - Université Paul SABATIER
9 avenue du Colonel Roche - Boîte postale 44346 - 31028 Toulouse Cedex 4
Tél. : 05 61 55 66 66 - Fax : 05 61 55 86 92

the University of Leiden (X. Tielens, H. Linnartz) recently performed some first measurements using a visitor ion trap on the DESIRS beamline. The last years we have also submitted a proposal to study the evolution of the branching ratio with energy using the linear trap available on DESIRS. Despite the novelty and interest of these studies in traps, progress is slow because the measurements are difficult (for instance time-resolved experiments would benefit from a higher VUV flux) but also because access to VUV beamlines is too limited. Our trap proposal was already delayed 3 times due to user oversubscription. This timing is difficult to reconcile with the very competitive contracts in which we are involved.

The Nanocosmos project

My team in Toulouse (IRAP and collaborators at LCAR, LCPQ and LAPLACE) is now committed to the ERC Synergy Grant project called Nanocosmos "Gas and dust from stars to the laboratory: exploring the Nanocosmos". This project is led in collaboration with two other principal investigators in Spain: J. Cernicharo and J. A. Martín-Gago (CSIC-ICMM, Madrid) and will run until mid-2020. Nanocosmos has the ambition to understand the formation and evolution of cosmic dust (including PAHs) by combining new strategies for astronomical observations, the development of millimetre receptors, innovative simulation chambers and astrophysical models. Studying the interaction with VUV photons of large carbonaceous molecules, carbon clusters and carbonaceous nanograins in general, will be one of the activities carried in the project by the Toulouse team.

Proposed developments at ALBA: Skiron VUV beamline and associated setups

The installation is of great interest for studies on photoionisation of molecules, the threshold for ionisation being ~7eV for singly ionised species and ~17 eV for doubly ionised. The key proposed apparatus is the magnetic-bottle-type time-of-flight electron spectrometer which combines large luminosity (~2π sr) as well as good energetic resolution. It is devoted to photoelectron measurement and allows multi-photoelectron coincidence like PEPECO (Photo Electron-Photo Electron Coincidence) for Photoelectron-Auger cascade correlation for example in atoms [10]. For molecules, the fast (multi)ionisation process is followed by a fragmentation process (the number of charged fragments gives the initial charge state of the molecule) and it is necessary to link the emitted photoelectrons with the charged fragments by a multicorrelation experiment (PE^nPI^mCO) to achieve a 'complete' description of molecular photoionisation. A mass-over-charge analysis is therefore necessary when dealing with PAH species. Therefore an upgrade including mass spectrometry is necessary to address our studies. The geometry of the magnetic bottle electron spectrometer proposed for the Skiron beamline suggests that the experimental set up described by Matsuda et al. [11] could be implemented.

We would also be very interested by the possibility to perform experiments in an ion storage device (ion trap or storage ring) but the performances of such setup should be first evaluated in details. One key parameter will be here the VUV photon flux that will be achieved on Skiron. We could contribute to this effort taking benefit from our experience with such setups.

Institut de Recherche en Astrophysique et Planétologie
CNRS - Université Paul SABATIER
9 avenue du Colonel Roche - Boîte postale 44346 - 31028 Toulouse Cedex 4
Tél. : 05 61 55 66 66 - Fax : 05 61 55 86 92

References

[1] West, B., Useli-Bacchitta, F., Sabbah, H., Blanchet, V., Bodi, A., Mayer, P.M., and Joblin, C., *"Photodissociation of Pyrene Cations: Structure and Energetics from $C_{16}H_{10}^+$ to C_{14}^+ and almost everything in between"*, J. Phys. Chem. A 118 (2014), 7824–7831

[2] Useli-Bacchitta F., Bonnamy A., Malloci G., Mulas G., Toublanc D., Joblin C., *"Visible photodissociation spectroscopy of PAH cations and derivatives in the PIRENEA experiment"*, Chem. Phys. 371 (2010), 16-23

[3] Simon A. and Joblin C., *"Photodissociation of $[Fe_x(C_{24}H_{12})_y]^+$ complexes in the PIRENEA set-up : iron-PAH clusters as good candidates for interstellar very small grains"*, J. Phys. Chem. A 113 (2009), 4878-4888

[4] West, B., Sit, A., Mohamed, S., Joblin, C., Blanchet, V., Bodi, A., Mayer, P. M., *"Dissociation of the Anthracene Radical Cation: A Comparative Look at iPEPICO and Collision-Induced Dissociation Mass Spectrometry Results"*, J. Phys. Chem. A (2014), sous presse

[5] West B., Joblin C., Blanchet V., Bodi A., Sztaryf B., and Mayer P.M., *"Dynamics of Hydrogen and Methyl Radical Loss from Ionized Dihydro-Polycyclic Aromatic Hydrocarbons: A Tandem Mass Spectrometry and Imaging Photoelectron-Photoion Coincidence (iPEPICO) Study of Dihydronaphthalene and Dihydrophenanthrene"*, J. Phys. Chem. A 118 (2014), 1807-1816

[6] West B., Joblin C., Blanchet V., Bodi A., Sztaryf B., and Mayer P.M., *"On the Dissociation of the Naphthalene Radical Cation: New iPEPICO and Tandem Mass Spectrometry Results"*, J. Phys. Chem. A 116 (2012), 10999-11007

[7] Martin S., Bernard J., Brédy R., Concina B., Joblin C., Ji, M., Ortega C. and Chen L., *"Observation of fast radiative cooling of Anthracene in a compact electrostatic storage ring"*, Phys. Rev. Lett. 110 (2013), id. 063003

[8] Mayer, P. M., Blanchet, V., Joblin, C., *"Threshold photoelectron study of naphthalene, anthracene, pyrene, 1,2-dihydronaphthalene, and 9,10-dihydroanthracene"*, J. Chem. Phys. 134 (24) (2011), 244312-244312-8

[9] Bréchignac, P., Garcia, G. A., Falvo, C., Joblin, C., Kokkin, D., Bonnamy, A., Parneix, P., Pino, T., Pirali, O., Mulas, G., Nahon, L., *"Photoionization of cold gas phase coronene and its clusters: Autoionization resonances in monomer, dimer and trimer and electronic structure of monomer cation"*, J. Chem. Phys. (2014), soumis

[10] Penent F., Palaudoux J., Lablanquie P., Andric L., Feifel R., and Eland J.H.D., *"Multielectron Spectroscopy: The Xenon 4d Hole Double Auger Decay"*, Phys. Rev. Lett. 95 (2005), 083002

[11] Matsuda A., Fushitani M., Tseng C.-M., Hikosaka Y., Eland J.H.D., Hishikawa A., *"A magnetic-bottle multi-electron-ion coincidence spectrometer"*, Review of Scien. Inst. 82 (2011), 103105

Institut de Recherche en Astrophysique et Planétologie
CNRS - Université Paul SABATIER
9 avenue du Colonel Roche - Boîte postale 44346 - 31028 Toulouse Cedex 4
Tél : 05 61 55 66 66 - Fax : 05 61 55 86 92

NEW YORK UNIVERSITY
DEPARTMENT OF CHEMISTRY
MOLECULAR DESIGN INSTITUTE

Bart Kahr, Professor
Phone: (212)992-9579
Fax: (212)992-7958

100 Washington Square East, Room 1001
New York, NY, 1003-6688
E-mail: bart.kahr@nyu.edu

5 October 2014

To the Skiron Beamline Evaluation Committee,

I am eager write in support of this exciting proposal.

The science of chiroptics, as described in the introduction to the proposal by Arteaga, Nicolás, and Ferrer, has a long and distinguished history. Most significantly, it gave us the very first evidence of the arrangements of atoms of in space. However, since these achievements in nineteenth century, determining structure/chiroptical property correlations has been a tale of woe. In large measure this is because average values of bisignate quantities like optical rotation and circular dichroism resist interpretation, and because these quantities ultimately arise in the complexity of electronic structure. We have recently shown that by choosing sufficiently simple molecules whose electronic structure is largely intuitive - non-enantiomorphous, planar conjugated hydrocarbons - the interpretation of optical activity becomes transparent.[1,2] However, matching these theoretical insights with experiment requires circular dichroism measurements at the very high energies to which the present proposal aspires; simple structures correspond to energetic excitations. For instance, we can now interpret the long wavelength optical activity from first principles but without extensive computation for cycloheptatriene. This is achieved by knowing which ultraviolet transitions are the strongest contributors. To match our theory with experiment we need to measure the rotatory power of the first excited state at around 280 nm. We can do this by making measurements on crystals of the related terpene, thujic acid, whose salts can easily be grown as chiral crystals. To match dienes by a similar strategy we need to reach absorption maxima below 200 nm. To match the first excitation energy of water (a long standing dream)[3] which would allow us to make CD measurements in ice XI we need to reach 168 nm. The ability to make such measurements is wholly dependent on the high energies available to Skiron and the sensitivity of the 4-PEM modulation scheme pioneered by PI Arteaga. There will be no equivalent capability anywhere else in the world.

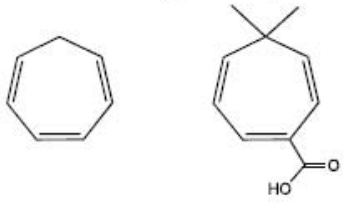

cycloheptatriene thujic acid

The Skiron photon intensity, 4-PEM sensitivity, and focused beam have other

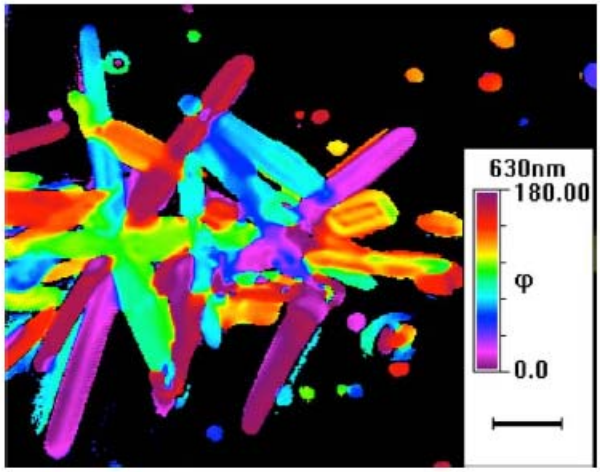

applications that are of considerable interest to us. Chiral anti-malarial drugs such as quinine and artemisinin, presumed to inhibit the crystallization of hemozoin in red blood cells thus increasing the concentration of parasite-killing free heme, must interact with the growth of hemozoin crystal faces enantioselectively. Understanding the inhibitory action of these drugs requires understanding their differential interactions with the mirror images faces of the centrosymmetric crystals. This necessitates, in turn, the abilitiy to distinguish crystals attached to the membrane of the food vacuole in red blood cells exposing their (100) or (-100) faces. To date, this has never been achieved for hemozoin, synthetic hemozoin (hematin) or any other crystal for that matter. It is commonly assumed that there is no way to distinguish the sense of an axial vector (the ± direction of the axis of a centrosymmetric crystal) with light. Herein, this can easily be established from the complete Mueller matrix deduced as described in the proposal. The figure shows the large synthetic hematin crystals and the map of the most absorbing direction. (Scale bar = 5 μ, collaborative study with P. Vekilov, University of Houston).

Please be well,

Bart Kahr

Bart Kahr

---

[1] Unpublished 2014. Murphy, V.; Kahr, B.

[2] V. L. Murphy, B. Kahr, Planar hydrocarbons more optically active than their isomeric helicenes, *J. Am. Chem. Soc.* **2011**, *113*, 2918–12921.

[3] C. Isborn, K. Claborn, B. Kahr, The optical rotatory power of water, *J. Phys. Chem. A*, **2007**, *111*, 7800-7804

8.- Acknowledgegments.

During the preparation of this project many persons have kindly contributed at different levels as clarifications, suggestions or ideas.
We would like to thank Laurent Nahon, Søren Vrønning , Josep M.. Ribo, Adolf . Canillas, Salvador Ventura, Javier Sancho, David Amabilino, Isaac Ciurans, Norbert Bowering, Cecilia Sanchez-Hanke, Carlos Escudero, Bonnie Wallace, Roberto Purrello, Angel Ureña, Cristobal Viedma, Joan Francesc Dulsat, Uwe Meierhenrich, Elies Molins, Christian Brouder, Ignasi Villaroya, Javier Garcia de Abajo and Oscar Matilla.

9.- References

[1] Comprehensive Chiroptical Spectroscopy vol 2. chapter 1, Edited by
N. Berova, P.L. Polavarapu, K. Nakanishi, R. W. Woody, J. Wiley and Sons inc. 2012

[2] V.L. Rosenfeld , Z. Physik, **52** , 161 (1928)

[3] A.S. Davydov, Theory of Molecular Excitons (translation), Mc Graw Hill NY 1962

[4] Comprehensive Chiroptical Spectroscopy vol 1.Edited by
N. Berova, P.L. Polavarapu, K. Nakanishi, R. W. Woody, J. Wiley and Sons inc. 2012

[5] Condon E. U. , Rev. of Modern Physics **9** , 432 (1937)

[6] See ref. 1 chap. 4.

[7] B. Ritchie , Phys. Rev A **13**, 1411 (1976)

[8] N. Böwering et al. , Phys. Rev. Lett. **86** 1187 (2001) and T. Lischke, Phys. Rev. A **70**, 022507 (2004)

[9] J. G. Lees,|, A. J. Miles, F. Wien1, and B. A. Wallace, Bioinformatics **22**, 1955, (2006)

[10] see ref. 6 chap. 8

[11] G. T. Carrol, M.M. Pollard, R. Van der Delden and B. L. Feringa. Chem.. Sci. 2010, **1** , 97

[12] H. Yoneda, Y. Nakashima and U. Sakaguchi, Chem. Lett. 1973 , 1343

[13] R. Breslow, Tetrahedron Letters 52 (2011) 4228–4232

[14] Wim L. et al. . Nature Chemistry 1, 729 (2009)

[15] see ref. 4 chap. 2

[16] S.N. Jasperson and S.E. Schntterly. Rev. Sci. Instr. 40, 761 (1969)

[17] See ref. 1 chap. 2.

[18] J.C. Sutherland, E.J. Desmond, P.Z. Takacs, Nucl. Instr. and Meth.: Phys. Res. 172 (1980) 195.

[19] P. A.. Synder and E. M. Rowe, Nuclear Instruments and Methods , **172**, 345 , 1980

[20] B.A. Wallace, et al., Nuclear Instruments and Methods in Physics Research A 649 (2011) 177.

[21] R. Hussainet al. , CHIRALITY 22:E149–E153 (2010)

[22] A. Giuliani et al. ,J. Synchrotron Rad. (2009). 16, 835–841
and M. Refregiers et al. J. Synchrotron Rad. (2012). 19, 831–835

[24] Laurent Nahon et al. ,J. Synchrotron Rad. (2012). 19, 508–520

[25] B. A. Wallace, Quarterly Reviews of Biophysics 42, 4 (2009), 317

[26] D. T. Clarke, A. J. Doig, B. J. Stapley, and G. R. Jones*Proc. Natl. Acad. Sci. USA* ,Vol. 96, pp. 7232–7237, June 1999

[27] B.M. Bulheller, A. Rodgerb and J. D. Hirst, Phys. Chem. Chem. Phys., 2007, **9**, 2020–2035

[28] O. Plekan, et al. **,** *J. Phys. Chem. A* **2007,** *111,* 10998-11005

[29] J. Martinez Ruiz, unpublished

[30] J. Jiang et al. *J. Phys. Chem. B* **2010**, *114*, 8270

[31] K. Gekko et al. *Chirality* **2006**, *18*, 329–334.

[32] P. M. Clayton et al. *Chirality* **2013**, *25*, 288

[33] L. Serrano- Andres et al. *J. Am. Chem. Soc.* **1998,** 120*,* 10912-10920.

[34] l. B. Clark *J. Am. Chem. Soc.* **1995**, *117*, 7974

[35] http://www.elettra.trieste.it/lightsources/elettra/elettra beamlines/cipo/cipobeamline.html

[36] S. Turchini et al. , Phys. Rev. A 70, 014502 (2004)

[37] H. Pauly, Atom , Molecule and Cluster Beams, Springer 2000

[38] D. Touboul et al. J. Chem. Phys. **138**, 094203 (2013)

[39] M. Tia et al. J. Phys. Chem. A 2014, 118, 2765−2779

[40] A. R. Al-Rabaa et al. Chem. Phys. Lett. 237 (1995) 480 and J. Phys. Chem. A, 101, 3273 (1997)

[41] M. Speranza et al. CHIRALITY 21:119–144 (2009)

[42] M. Faubel et al. J. Chem. Phys. **106** (22), 1997

[43] B. Winter et al. Chem. Rev. 2006, 106 , 1176

[44] M. A. Brown et al. Annu. Rep. Prog. Chem., Sect. C, 2009, 105, 174

[45] B. Winter Nuclear Instruments and Methods in Physics Research A 601 (2009) 139

[46] J. Schellman, et al., *Chem. Rev*. 87(6) (1987): 1359-1399 (1987).

[47] O. Arteaga, "Mueller matrix polarimetry of chiral anisotropic media", PhD Thesis, (2010).

[48] N. Berova, et al., "Comprehensive Chiroptical Spectroscopy", vols. I and II, John Wiley, New Jersey (2012).

[49] O. Arteaga et al., *Chim. Ogg.* 30(5), 6-9 (2012).

[50] A. D. Miller et al., "Essentials of Chemical Biology. Structure and Dynamics of Biological Macromolecules". John Wiley, New Jersey (2013).

[51] T. Troxell, et al, *Macromolecules* 4, 519-527 (1971)

[52] D. H. Goldstein, "Polarised Light", Marcel Dekker, New York (2003).

[53] R. A. Chipman, "Polarimetry", chapter 22 in Handbook of Optics II, 2nd Ed, McGraw-Hill, 1995.

[54] O. Arteaga, *Opt. Lett*., 38(7), 1131-1133 (2013).

[55] R. Ossikovski, *Opt Lett.*, 36(12), 2330-2332 (2011).

[56] R. Ossikovski et al., *Opt. Lett.*, 39(15), 4470-4473 (2014).

[57] C. Meinert, et al., *Angew. Chem. Int. Ed.* 2012, 51, 4484-4487

[58] R. Kuroda, et al., *Rev. Sci. Instr.*, 72, 3802-3810 (2001).

[59] R. Kuroda, et al. in "Comprehensive Chiroptical Spectroscopy", John Wiley, New Jersey, I, 91-114 (2012).

[60] A. J. Miles, *Chem. Soc.* Rev. 35(1), 39-51 (2006).

[61] N. J. Greenfield, *Nat Protoc.* 1(6), 2876-2890 (2006).

[62] B.M. Bulheller et al., *Phys. Chem. Chem. Phys.*, 9, 2020–2035, (2007)

[63] B. A. Wallace, *Quat. Rev. Biophys* 42(4) 317–370 (2009).

[64] a) J. G. Lees et al., *Bioinformatic*s 22, 1955-1962. (2006) b) A. J. Miles et al., *Chem. Soc. Rev.*, 35, 39–51 (2006).

[65] J. H. Burnett, et al., *Phys. Rev. B*, 64, 241102 (2001).

[66] Garton, W. R. S., et al. " *J Phys B: Atom Mol Phys*, 16, 389 (1983).

[67] A. Gupta et al. "Reinvestigation of electric Field-Induced Optical Activity in a-Quartz: application of a polarimeter with four photoelastic modulators", *Chirality* in press 2013

[68] V. G. Čigrinov, Vladimir G. *Electrooptic effects in liquid crystal materials*. Springer, (1996).

[69] O. Arteaga et al *Appl. Opt.* 51(28) 6805-6817 (2012).

[70] B. Norden et al., *Quat. Rev. Biophys*. 25(1), 51-170 (1992)

[71] R. Adachi, et al., *J. Biol. Chem.,* 282, 8978–8983 (2007)

[72] Jin, Lee-Way, et al. *PNAS* 100(26), 15294-15298 (2003):

[73] M. Rittman, et al. *Phys. Chem. Chem. Phys.*, 14(1), 353-366 (2012).

[74] M. R. Hicks, et al., *J. Mol. Biol.* 383, 358-366 (2008).

[75] A. Rojas, et al., *J. Am. Chem. Soc*. 135(32), 11975-11984 (2013).

[76] O. Arteaga, et al., *Thin Solid Films* 519(9), 2617-2623 (2011).

[77] C. Y. Han, et al., *Rev. Scient. Inst*. 77, 023107 (2006)

[78] P. Gleyzes, et al., *Opt. Lett.* 22, 1529-1531 (1997)

[79] O. Arteaga, et al., *ChemPhysChem* 11(16), 3511-3516 (2010).

[80] Wigglers, Undulators and their applications. H. Onuki and P. Ellaume , Taylor and Francis 2003, chap 4.

[81] E. Pereiro et al. J. Synchrotron Rad. (2009). 16, 505–512

[82] T. Lischke et al. Phys. Rev. A 70, 022507 (2004)

[83] D. Derera et al. Jour. of Electr. Spectrosc. and Related Phenomena 195 (2014) 109

[84] P. Kruit at al. J. Phys. E: Sci. Instrum., Vol. 16. 313 (1983)

[85] H. Handschuh et al. Rev. of Sci. Instruments 66 (1995) 3838

[86] A. Kothe et al. Rev. of Sci.Instruments **84**, 023106 (2013) and F. Buchner et al. ibid. 81, 113107 (2010).

[87] G. Prumper et al. Phys. Rev. A 69, 062717 (2004)

[88] A. Derossi, F. Lama, M. Piacentini, T. Prosperi, N. Zema, Rev. Sci. Instrum. 1995, 66, 1718.

[89] M.R. Weiss et al. Nuc. Instrum. and Methods in Physics Research A 467–468 (2001) 449–452

[90] J. Raabe et al. Rev. Sci. Instrum. **79**, 113704 (2008)

[91] R. Renninger et al. unpublished report

[92] Usher et al. Jour. of Appl. Physics 98, 064102 (2005)

[93] T. C. Oakberg, et al. *Proc. SPIE 4133, Polarization Analysis, Measurement, and Remote Sensing III*, 101 (2000).

[94] K. Gekko et al. *Chirality* **2006**, *18*, 329–334

[95] I. Ciurans, private communication